



BENEMÉRITA UNIVERSIDAD AUTÓNOMA DE PUEBLA

FACULTAD DE CIENCIAS FÍSICO MATEMÁTICAS

LICENCIATURA EN FÍSICA APLICADA

Study of the event plane
resolution
in Au-Au collisions with the
Beam Monitor Detector of
MPD-NICA at JINR

Tesis presentada para obtener el grado de: Licenciatura en
Física Aplicada.

Presenta:

Valeria Zelina Reyna Ortiz

Director:

Dr. Mario Rodríguez Cahuantzi

Puebla, México

Diciembre 2018

ABSTRACT

There are two important observables in heavy ion collisions: *the impact parameter and the event plane resolution*.

The reaction plane, is a plane made from the direction of the impact parameter (x-axis) and the beam direction (z-axis). Experimentally, the event plane that is measured is an approach to the reaction plane.

The aim of this thesis is to obtain the event plane resolution, using the Beam on Beam Monitoring Detector (BE-BE) of the MexNICA collaboration for the Multipurpose Detector (MPD) experiment of NICA at the Joint Institute for Nuclear Research (JINR), it consists of two detectors: BE-BE A and BE-BE C each one located 2 meters apart on both sides of the interaction spot along the beam pipe.

The inclusion of a detector capable to monitor the beam activity is desirable in collider experiments, during commissioning or regular operations. With the information provided with the detector, it could be possible to setup a trigger system to identify and discriminate beam-beam minimum bias or centrality events from background and beam-gas interactions. In addition, these types of systems can be used to aid the reconstruction of physical observables of interest in heavy-ion collisions.

To determine the event plane resolution, a macro analysis was created using the MPD Root framework, to analyze Au-Au collisions were analyzed at $\sqrt{S_{NN}} = 9$ GeV.

We found that for events between 25% and 50% of centrality the event plane resolution is near the 50%.

The results of this work had been presented in:

- *LXI Congreso Nacional de Física y V Congreso Latinoamericano de Física* From 7th 12th of october 2018, in Puebla, Pue.
- *XVIII Mexican School of Particles and Fields (MSPF)* and *2018 University of Sonora School of High Energy Physics (USHEP)* in Hermosillo, Sonora, from the 21st to the 27th of October 2018.
- *General MexNICA Meeting. After the 2nd Collaboration Board Meeting of MPD-NICA*, 15 & 16 of November, at Ecocampus BUAP, Puebla. <https://indico.nucleares.unam.mx/event/1437/>

-
- Summer Student Program 2018 at JINR. Under the supervision of Dr. Vyatcheslav Golovatuyk. See: [17]
 - Some of the results can be found also in *A beam-beam monitor detector for the MPD-NICA experiment at JINR* arXiv:1809.10553 [2]

Key Words: Particle detectors, heavy ion collisions, MPD, NICA, beam monitoring.

DEDICATION AND ACKNOWLEDGEMENTS

To my parents. Who had to struggle with the fact of having a daughter that wanted to study something weird and unknown for them, with dreams and stories that always seemed crazy, with ideas completely out of the world they lived in; and the habits, manners, and talks that changed and got crazier across the years; but still, they stayed by her side. Hey mom, hey dad... about that "Crazy thing that I decided to study", here it is. Thanks for staying.

To my little sister, who still believes that I'm really weird, and will give me a special look every time I talk about physics. But she doesn't care about it, she embraces it.

To my dear best friend Andrea, the person who never left my side. For all your support, advises, help and the years of friendship. Thanks.

Thanks to the Mexican workers who through their contributions make possible the development of basic and applied science in Mexico.

Special thanks and acknowledges to Proyecto VIEP: 100524451/VIEP2018. And computer resources, technical advise and support provided by Laboratorio Nacional de Supercómputo del Sureste de México (LNS), a member of the CONACYT national laboratories, with project No.53/Primavera 2017.

To the organizing committee of the Summer Student Program at the Joint Institute for Nuclear Research (JINR) for choosing me for the 2018 edition. Special mention to Dr. Vyatcheslav Golovatyuk, who welcomed me to Dubna, and the NICA project. This experience changed my life.

To all the people I met in Dubna, everyone showed how big and amazing the world is, how different we are from each other, and how similar we could be, there will always be a part of each one of them in me; you all saved me from something that you didn't know that it was there, I will thank you forever. But, specially to my dear *Betânia*, my non-related sister from Brazil, although I still cannot pronounce your name; you taught me how does strength looks like. And inspired me to keep going forward.

Thanks to the guys from "Del Aula al Universo", I've been in this project the whole career, and it helped grow as professional and person. Thanks to professor Rogelio, leader of this project, for believing and trusting in me.

TABLE OF CONTENTS

	Page
List of Tables	ix
List of Figures	xi
1 Introduction	1
1.1 The Standard Model	1
1.2 The Quarks Model	3
1.3 Quantum Chromodynamics	5
1.3.1 Quark Gluon Plasma	7
1.4 Heavy Ion Collisions	9
1.4.1 Impact Parameter	9
1.4.2 Anisotropic flux	10
1.4.3 Event plane	12
2 The NICA and the MPD Experiment	15
2.1 The NICA project at JINR	15
2.2 The MPD experiment	18
2.3 The Beam Monitoring Detector	19
2.3.1 The MexNICA collaboration	19
2.3.2 Geometry	20
3 Software for the analysis	23
3.1 ROOT	23
3.2 MPD-ROOT	24
3.3 Macro	24
4 Results	25
4.1 Multiplicity	25
4.1.1 Hodoscope Geometry	31
4.2 Event plane	36
4.2.1 Vector Q calculus	37

TABLE OF CONTENTS

4.2.2	Calculus of the event plane angle.	37
5	Conclusions	41
A	Appendix A	43
A	Appendix B	45
A	Appendix C	53
	Bibliography	55

LIST OF TABLES

TABLE	Page
1.1 Leptons classification according to their quantic numbers	2
1.2 Quarks classification according to their quantic numbers	2
1.3 Fundamental forces of nature and their classification as the S.M says	2
4.1 Fundamental forces of nature and their classification as the S.M says	38
A.1 Results of σ	53
A.2 Results of σ	54

LIST OF FIGURES

FIGURE	Page
1.1 The elementary particles of the Standard Model. Image taken from: https://www.physik.uzh.ch	3
1.2 Quarks Triplet	4
1.3 Flavor conservation diagram	7
1.4 Phase diagram plot of hadronic matter to QGP.	8
1.5 Impact Parameter representation. Taken from https://www.researchgate.net	10
1.6 Diagram of the Reaction plane.	11
2.1 A picture of NICA. It is shown the three experiments and the rest of the components. Image taken from http://nica.jinr.ru/complex.php	17
2.2 Phase diagram of hadronic matter and QGP. There is a critical point in the temperature T_c in which the quarks and gluons are not confined. In the same way there is a critical point N_c for the baryonic density from which quarks and gluons are not confined. The curved line between the critical points refers the phase transition between these both states.	17
2.3 A picture of MPD. Image taken from http://nica.jinr.ru/complex.php	18
2.4 General view of the MPD-NICA http://nica.jinr.ru/complex.php	19
2.5 The Hybrid detector geometry	20
2.6 The Hodoscope detector geometry	21
4.1 This figure shows the distribution of Kinematics, at the simulation with the BE-BE detector at both sides of the interaction point.	26
4.2 a) Hits Distribution for all the particles. b) Hits distribution only for primaries	27
4.3 a) Momentum vs CellID for all the particles. b) shows Momentum vs CellID only for primaries	28
4.4 The a) plot shows the Time vs Cell ID for all the particles. The b) plot shows only for primaries	29
4.5 Multiplicity VS Cell ID	30
4.6 The a) plot shows a graph of Number of entries vs Multiplicity of each of the rings of the Hybrid proposal. The b) plot shows the Number of entries vs Multiplicity for each ring independently.	31

4.7	a) Shows the Hits Distribution for all the particles. b) Shows only for primaries	32
4.8	The a) plot shows the Momentum vs CellID for all the particles. The b) plot shows only for primaries	33
4.9	The a) plot shows the Time vs Cell ID for all the particles. The b) plot shows only for primaries	34
4.10	Multiplicity VS Cell ID	35
4.11	The a) contains all the plots of each of the rings of the Hodoscope Geometry proposal, all the six of them are overlaped. b) Contains the same plots but shown individually.	36
4.12	The first three rings of the BE-BE detector with the Cell ID.	37
4.13	Estimated event plane resolution with BE-BE detector.	39
A.1	a) Hits Distribution for all the particles at 11 GeV. b) Hits distribution for 9MeV. . . .	46
A.2	a) Hits Distribution for primary particles at 11 GeV. b) Hits distribution for 9MeV. . .	47
A.3	a) Momentum vs CellID plot for all the particles at 11 GeV. b) for 9MeV.	48
A.4	a)Momentum vs CellID plot for primary particles at 11 GeV. b) Hits distribution for 9MeV.	49
A.5	a) Time of Flight plot for all the particles at 11 GeV. b) Hits distribution for 9MeV. . .	50
A.6	a) Time of Flight plot for primary the particles at 11 GeV. b) Hits distribution for 9MeV.	51
A.7	a) Hits Distribution for all the particles at 11 GeV. b) Hits distribution for 9MeV. . . .	52

INTRODUCTION

The main goal of high energy physics is to study and understand what are the most important and fundamental blocks of matter, and how does the interaction between them works. In the years ahead of us, physics holds a great promise to answer important questions like: What is the origin of matter and anti-matter? What does a non-confined state of nucleons looks like? What happened just right after the Big Bang? Are all the universe forces unified into one force at high energy?

1.1 The Standard Model

The Standard Model (SM) is a theory that describes the fundamental forces of the universe, the weak, strong and electromagnetic force, as well as the elementary bricks that constitute matter: leptons and quarks.

Leptons are particles classified in three generations as shown in Table 1.1, there are six leptons and they are classified according to their quantic numbers (charge Q , quantum number of the electron L_e , muonic number L_μ and tautonic number L_τ). There also exist the antiparticles, with the opposite sign.

For *quarks*, there are six different flavors: *up, down, strange, charm, top, bottom*. Also they have their corresponding antiparticles. The quarks are also divided in three generations.

According to the statistics there is a way to classify particles: *Fermions* and *Bosons*.

Fermions obey Fermi-Dirac statistic, also they obey the Pauli exclusion principle, they have a half spin.

[H]

	l	Q	L_e	L_μ	L_τ
1st generation	e	-1	1	0	0
	μ	0	1	0	0
2nd generation	μ	-1	0	1	0
	ν_μ	0	0	1	0
3rd generation	τ	-1	0	0	1
	ν_τ	0	0	0	1

Table 1.1: Leptons classification according to their quantic numbers

	q	Q	d	u	s	c	b	t
1st generation	d	$\frac{1}{3}$	-1	0	0	0	0	0
	u	$\frac{2}{3}$	0	1	0	0	0	0
2nd generation	s	$\frac{1}{3}$	0	0	-1	0	0	0
	c	$\frac{2}{3}$	0	0	0	1	0	0
3rd generation	b	$\frac{1}{3}$	0	0	0	0	-1	0
	t	$\frac{2}{3}$	-1	0	0	0	0	1

Table 1.2: Quarks classification according to their quantic numbers

The **Bosons** obey the Bose-Einstein statistic, but not the Pauli exclusion principle; they have a complete spin. In the bosons groups exists the Higgs Boson, the particle responsible of providing mass to other particles.

All the interactions have a mediator, there are four fundamental forces in nature, each one of them has their own mediator. According to the standard model there are twelve mediators, eight of them are gluons, this mediators are: strength force mediator, photon for the electromagnetic force, and W^\pm and Z bosons for the weak force. The gravitational force is not included, although in theory it has a mediator named *graviton*. See Table 1.3. [10][8]

Force	Reach	Theory	Mediator
Electromagnetic	10^{10-2}	Electrodinamic	Photon
Weak	10^{-13}	Electroweak	W^\pm, Z
Strong	10	Quantum Cromodynamics	Gluons

Table 1.3: Fundamental forces of nature and their classification as the S.M says

There also exist heavy particles, that are composed by quarks, they are named *Hadrons*. This kind of particles is divided in two clases as the Standar Model says: *Baryons* and *Mesons*.

Baryons, are fermions, since the obey the Fermi-Dirac statistic and have a $\frac{1}{2}$ or $\frac{3}{2}$ spin, they are

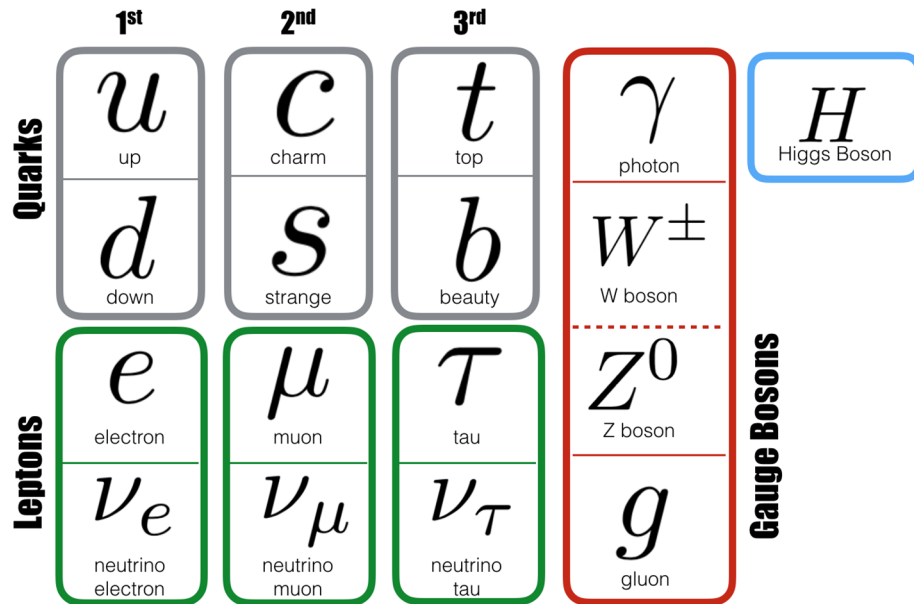


Figure 1.1: The elementary particles of the Standard Model. Image taken from: <https://www.physik.uzh.ch>

composed by quarks. The anti-baryons are composed by three antiquarks and three different anticolors. They group nucleons and non-stable particles with bigger mass than the ones of the nucleons, called, hiperons, like $\Delta, N^+, \Sigma, \Omega$.

Mesons, in other hand obey the Bose-Einstein statistic and have a spin 0 or 1, that means they are bosons. This same group includes mesons π also called *pions*, mesons K or *kaons*, and mesons η , there are many more mesons in this group and they depend on the flavor of the quark and the anti-quark that compose them.

The Standard Model is one of the most important theories in High Energy Physics field; experimentally no contradictions have been detected to the model. In 2013 the existence of the Higgs Bosson was verified in the LHC of CERN.

1.2 The Quarks Model

Hadrons are made from quarks, to understand the properties of this particles, the incorporation of *Group theory*, was important. The first three quarks were predicted and found experimentally, this ones were the *up, down, strange* (u, d, s) quarks, they were found forming an eight-fold path of a triangle shape (Figure 1.2). More particles were found with different characteristics, like the existence of other three quarks was found, the *beauty, charm and top* (b, c, t), with six different flavors and their respective antiparticles.

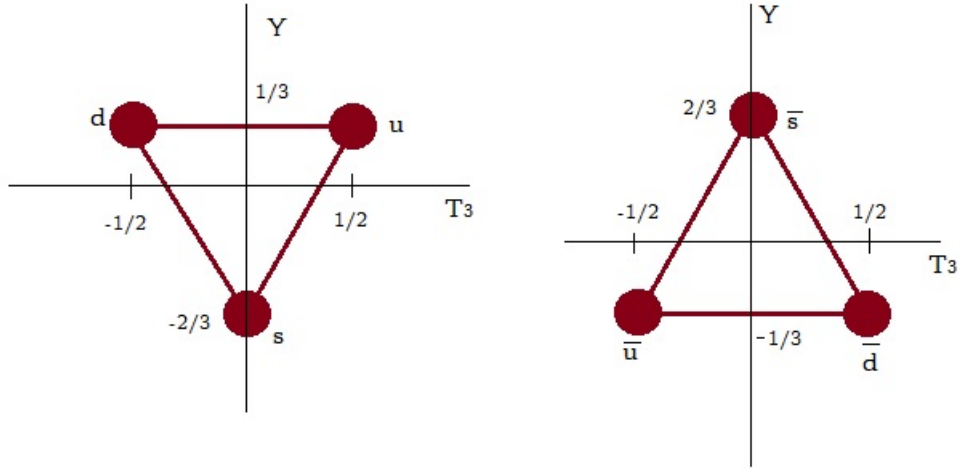


Figure 1.2: Quarks Triplet

From table 1.2, quarks have an fractional electric charge, that can be expressed with the equation: $Q = I_3 + \frac{N_B+S}{2}$, where, Q is the electric charge, I_3 is the the third iso-spin component, N_B is the baryonic number and S is the strangeness. The sum of $N_B + S$ is called *hipercharge* Y . Baryons are made from three quarks and each one of them has a baryonic number $N_B = \frac{1}{3}$. To make a quark combination that could form a baryon, we will need adequate values of spin, charge and strangeness. [10]

The number of possible combinations for the three quarks of different flavors is 27, but, there are restrictions based of the symmetry. Example, Ω^- , Δ^- and Δ^{++} are made from the sss , ddd and uuu respectively, this is the reason why they have a symmetry of low interchange of any pair of quarks, and this property must be present in every baryon. In case of having a ddu the complete state is express by the equation 1.1 which is symmetric under the interchange of any pair of quarks.

$$(1.1) \quad \frac{1}{\sqrt{3}}(|ddu\rangle + |udd\rangle + |dud\rangle)$$

From the symmetric combinations, we can obtain only 10 of them that could agree with the symmetry, of the seventeen remaining states only one is completely asymmetric:

$$(1.2) \quad \frac{1}{\sqrt{6}}(|dsu\rangle + |uds\rangle + |sud\rangle - |usd\rangle - |sdu\rangle - |dus\rangle)$$

All of the other combinations are made from a linear combination between a symmetric and asymmetric one, and can be expressed as:

$$(1.3) \quad |uud\rangle_S = \frac{1}{\sqrt{6}}(2|uud\rangle - |duu\rangle - |udu\rangle) \quad |uud\rangle_A = \frac{1}{\sqrt{2}}(|udu\rangle - |duu\rangle)$$

For mesons, we only need one quark and one anti-quark, because the baryonic number is equal to zero.

When the particles were ordered in the different octuple paths, Ω^+ were predicted, this particle had not been measured experimentally and this theory said that these particles should have been made from three quarks s , which was clearly a big contradiction, since the quarks had been classified as fermions. An important question was made in that moment: *How was it possible that there was more than one particle in the same state?*. The Ω^- was found in 1964, physicists of the time were in charge of a restructuring of the theory and decided to give another property to the quarks; the *color*, red, green and blue, with this it was possible to reestablish a spin-statistic connection, from then, it was established that baryons were made from identical fermions, and they must have a wave function that is completely anti-symmetric under the interchange of any pair of constituent quarks. Let Ψ be the wave function of a baryon. [10].

$$(1.4) \quad \Psi(1,2,3) = \Phi_{space}(\vec{r}_1, \vec{r}_2, \vec{r}_3) \chi_j(1,2,3) \xi_1(1,2,3) \Psi_{color}(1,2,3),$$

where χ is the spins wave function and ξ_1 is the wave function of the flavor and Ψ_{color} is the form of the singlete.

$$(1.5) \quad \Psi_{color}(1,2,3) = \frac{1}{\sqrt{6}}(|rgb\rangle + |gbr\rangle + |brg\rangle - |grd\rangle - |bgr\rangle - |rbg\rangle),$$

then, a hadron is known to be *white*, when the color charge is on balance. There is a theory that studies this property in a more extensive way, this is *Quantum Chromodynamics* or QCD.

1.3 Quantum Chromodynamics

This Quantum Chromodynamics theory studies and describes one of the fundamental forces of physic, the strong force. This theory also studies the shape in which the hadrons are constituted, that are made from quarks. The strong force is mediated by gluons, that are interchanged by the

quarks when an interaction occurs. The main responsible of this interaction is the color charge. The range of the cromodynamic force is measured by the coupling constant:

$$(1.6) \quad g_s = \sqrt{4\pi\alpha_s},$$

where α_s can take different values depending on the spaces between interacting particles, in anyway it is considered a coupling constant.

The nuclear force gets stronger as the distances increment, but it gets weaker when the distances are short, this is called *asymptotic freedom*, this means that the quarks have a *free* behavior inside the hadron. The scope between quarks and gluons depends on the interaction conditions; so in the QCD the coupling constant has a relation with the moments transfer q given by:

$$(1.7) \quad \alpha(q^2) = \frac{\alpha_0}{1 + \alpha_0 \frac{33-2n_f}{12\pi} \ln \frac{-q^2}{\mu^2}},$$

where α_0 is the coupling constant for the transfer momentum μ and n_f is the number of flavors. When the distance between two quarks is really short, the intensity of the interactions lows down. This explains why, when the quarks are really near, there exist the asymptotic freedom. One of the most important ways to study this behavior is study the evolution of the coupling constant in respect of the energy of the process. For QCD, this parameter has to low down when the energy rises. [11]

There is also the flavor conservation, that says, that the color of a quarks can change, but not its flavor. Example, at an interaction of a u flavored quark with a red color u_r and another quarks with u flavor and blue color u_b we will obtain a $g_{g\bar{r}}$ gluon, and as result a u_r quark and a u_b quark 1.3. This means the flavor always maintains as well as the electric charge, which means that the gluon will balance any change on the quarks, due to the fact that the gluon possesses a positive color charge and a negative color charge:

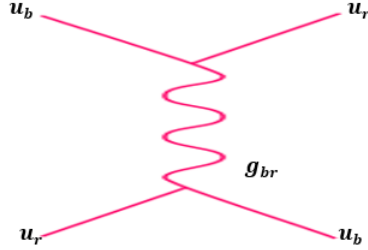


Figure 1.3: Flavor conservation diagram

$$\begin{aligned}
 |1\rangle &= (r\bar{b} + b\bar{r})/\sqrt{2} \\
 |2\rangle &= -i(r\bar{b} - b\bar{r})/\sqrt{2} \\
 |3\rangle &= (r\bar{r} - b\bar{b})/\sqrt{2} \\
 |4\rangle &= (r\bar{g} + g\bar{r})/\sqrt{2} \\
 |5\rangle &= -i(r\bar{g} - g\bar{r})/\sqrt{2} \\
 |6\rangle &= (b\bar{g} + g\bar{b})/\sqrt{2} \\
 |7\rangle &= -i(b\bar{g} - g\bar{b})/\sqrt{2} \\
 |8\rangle &= (r\bar{r} + b\bar{b} - 2g\bar{g})/\sqrt{6}
 \end{aligned}
 \tag{1.8}$$

This interactions do not only happen between quark-gluon-quark, but also between gluon-gluon since they have a color charge they can interact between themselves.

We already mentioned that the hadron color is white if we balance the color, this is because this particles are color singletes.

1.3.1 Quark Gluon Plasma

At high temperatures and energy densities, Quantum Chromodynamics predicts a phase transition where quarks and gluons behave freely, this state is known as *Chromodynamic Matter* or *Quark Gluon Plasma* (QGP). The theory says, that right after the Big Bang, at a time of $10^{-5}s$, the universe was all made of QGP, and when it started to expand and cool down, there was another phase transition called *Hadronization* in which the gas of hadrons was made, and finally nuclear matter. (See figure 1.4).

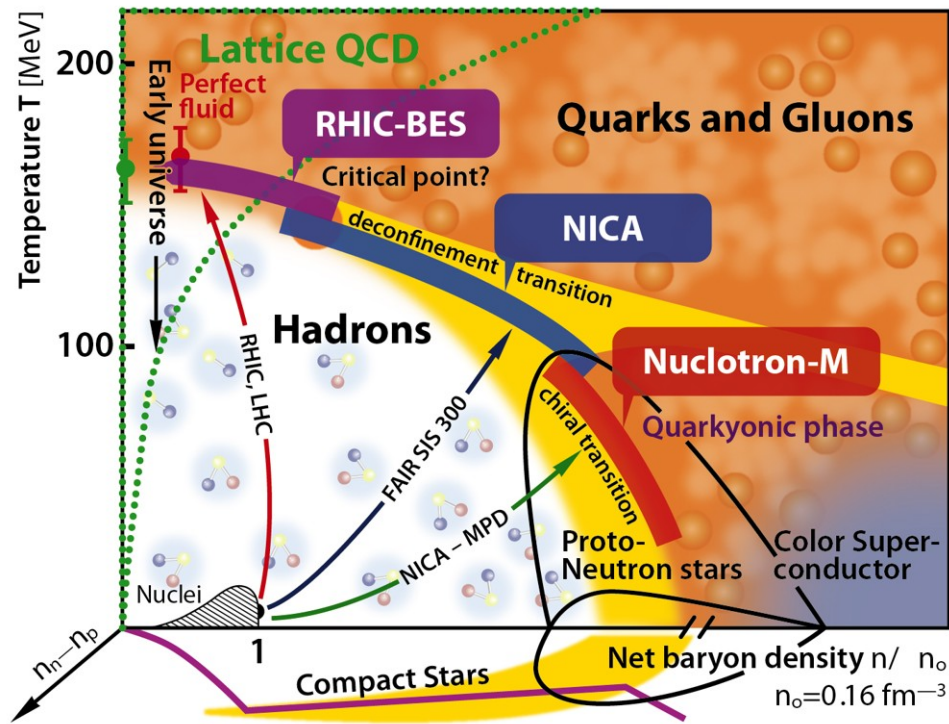


Figure 1.4: Phase diagram plot of hadronic matter to QGP.

Up to this day, some of the characteristics of matter when we approach to this limits of temperature and energy density had been found.

Hadrons have a radio and a volume needed for they to exist $V_h \simeq (4\pi/3)r_h^3$ where $r_h = 1fm$ is the radio of the hadron. This makes the density limit of hadronic matter n_c like:

$$(1.9) \quad n_c = \frac{1}{V_h} \simeq 1.5n_0,$$

where $n_0 = 0.17fm^{-3}$, and is the density of the normal nuclear matter.

Hadronic interactions happen to bring with themselves a high production of resonance; and the resulting number, (m), of hadron species grows exponentially as the function of mass of resonance $m, \rho(m) \sim exp(bm)$. In the thermodynamics of hadrons, this exponential grows in the degeneration of the resultant resonances, in the upper limit of the temperature of hadronic matter with $T_c = 1/b \simeq 150 - 200MeV$. Hadrons have a neutral color charge when located above the T_c limit in the QCD. The hadronic matter, then, is made by colored components of hadronic dimensions, at really high temperatures and densities matter could transform into QCP. The quarks and gluons then would be in a free state, and a phase change would occurs from a state of

conduction of color charge.[20]

There is also a phase transition with respect of the mass and the constituents of hadronic matter when $T = 0$ in vacuum. Quarks look like gluons when they are hadronized. With this the mass of those kind of quarks is $m_q \sim 0$ which is replaced by the mass of the constituent quark $M_q \sim 300MeV$. In a really hot medium there is a non-confinement state of hadrons $M_q \rightarrow 0$. For $m_q = 0$ there exist a quiral symmetry, $M_q \neq 0$ this implies the rupture of the mentioned symmetry, and at high temperatures $M_q \rightarrow 0$ the symmetry is restored.

1.4 Heavy Ion Collisions

Gluons thermalize really quick and form QGP, also the energetic partons traverse this plasma and form a shower of particles called *jets*. If we analyze the final particles in a variety of different ways we can study the properties of QGP and the dynamics of multi-scale processes in QCD, which rules its formation and evolution, providing what is the simplest form of complex quantum matter known by man. [4]

One of the most important characteristics of heavy ion collisions is the energy of the process. When a big fraction of energy is deposited in a really small space in a short time, the density could be really big. The magnitude of the energy involved in the collisions of nuclei-nuclei will allow us to have this phenomena.

In nuclei collisions, effective section is highly large and inelastic. The two nuclei of this kind of collision lose a big part of their energy, which is deposited in the neighborhood of the mass center and is carried by pions and mesons that come out of the collision. In central collisions there are many inelastic collisions between nucleons, where the energy density turns to be high enough to reach energies of the order of GeV/fm^3 ; this is needed to reach the state where the formation of matter like the quark-gluon plasma occurs. [9]

Ultra-relativistic heavy-ion experiments have been performed at the Brookhaven Alternating Gradient Synchrotron (AGS), the CERN Super Proton Synchrotron (SPS) and the Brookhaven Relativistic Heavy Ion Collider (RHIC) with maximum center of mass energies of $\sqrt{s_{NN}} = 4.75$, 17.2 and 200 GeV respectively. The Large Hadron Collider (LHC) at CERN has commissioned for Pb+Pb collisions at an energy above $\sqrt{s_{NN}} = 5.5 TeV$. [3]

In this section we explain what are the necessary variables for the study of heavy ion collisions.

1.4.1 Impact Parameter

Lets call A and B, the nuclei of a collision. We call *Impact parameter* b to the distance between from the center of A to the center of B. When the collision is central $b = 0$, but if the collision is

peripheral $b > 0$.

If we want to determine the impact parameter of a collision we need another variable, this is because it is not possible to measure directly this distance. The variable needed is the Event Multiplicity M . The multiplicity shows the number of particles generated during the collision.

So, when the multiplicity is a number greater than zero: $M \gg 0$ then the impact parameter is $b \rightarrow 0$; and when $M \rightarrow 0$ then $b > 0$.

The existence of an interaction between two nuclei has a probability that depends on their area:

$$d\sigma(b) = 2\pi b db$$

[3]

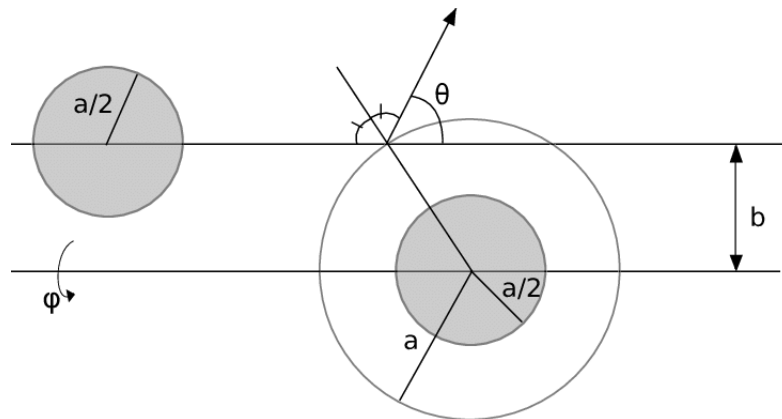


Figure 1.5: Impact Parameter representation. Taken from <https://www.researchgate.net>

1.4.2 Anisotropic flux

The most common way to visualize the flux of a collision is to imagine it like a *fireball*, that expands radially. When two nuclei collide there is a generation of primary particles that, in their trajectory have re-dispersion and create a particles flux that expands in time. In peripheral collisions this flux is anisotropic, and has a preferential direction. In figure 1.6 we can see a representation of a peripheral collision, the volume of the interaction has a shape similar to and "almond", this one is called the *participant* and the non-interacting parts are called *spectators*.

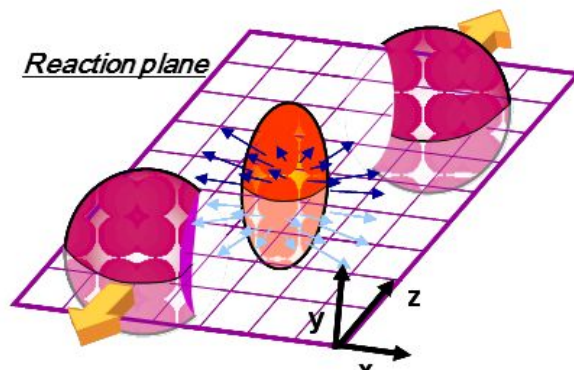


Figure 1.6: Diagram of the Reaction plane.

The anisotropic flux is a name use to described the collective evolution of the system. [9]

The anisotropic flux is described in terms of the gradient of pressure that is directly related with the state equation of the system, this is why, if we study the flux of a system, we obtain an important tool to characterize the interaction system that was created in a heavy ion collision. The flux can be of two different shapes: one that expands radially, and the anisotropic one; the first one affects the termic spectrum of the final state of the particles, and the second affects the spacial orientation of the particles momentum.

In heavy ion collisions, the shape and size of the collisions region depend on the *impact parameter*, (the distance between the centers of the colliding nuclei in the transverse plane). Then the plane that is formed in direction of the impact parameter \mathbf{b} and the beam direction is known as the *reaction plane* (see figure 1.6).

In non central collisions the azimuthal distribution of the final state of the particles is completely anisotropic. This is the reason why we can calculate the reaction plane, with respect of which the distribution of the momentum of the particles shows a strong dependence to $\cos(n[\phi - \Psi_R])$. Where ϕ is the azimuthal angle with respect of the viewer, and Ψ_R is the angle of the reaction plane.

When the collision is non-central, the impact parameter is different from zero, the region of the reaction is not spherical. The re dispersion of the constituents in the system of the collision convert the initial coordinates of the anisotropic space to coordinates of momentum-space anisotropic, while the gradient of the pressure is not symmetric. The anisotropic flow is quantified by the coefficients in the Fourier decomposition of the azimuthal angular particle distribution. If the particle azimuthal angle is measured with respect to the direction of the reaction plane then it leads to: [21] [3]

$$(1.10) \quad E \frac{dN}{d^3p} = \frac{1}{2\pi} \frac{dN}{p_T d p_T d \eta} \left(1 + 2 \sum_{n=1}^{\infty} v_n(p_T, \eta) \cos[n(\phi - \Psi_R)] \right),$$

where E is the particle's energy, N is the yield, p is the total momentum, p_T is the transverse momentum, ϕ is the azimuthal angle, and η the pseudorapidity, and Ψ_R is the reaction plane angle corresponding to the n^{th} -order harmonic v_n .

The Fourier coefficients v_n are given by:

$$(1.11) \quad v_n = \langle \cos[n(\phi - \Psi_R)] \rangle,$$

where the mean goes over all the events.

For odd harmonics v_n changes of sign depending on the rapidity $\pm y$, this is due to, the distribution of particles is the same inside both hemispheres but opposite sign for the moment conservation.

1.4.3 Event plane

The *reaction plane* Ψ_R is an important observable for the reconstruction of any event. This plane is composed by the impact parameter and the beam direction, as shown in Figure 1.6:

The reaction plane cannot be measured directly in an experiment, but we can determine the *event plane*.

This plane is consequence of eq. 1.10, replacing Ψ_R of the reaction plane with the event plane angle Ψ_n . Where n is the harmonic used in the calculus. [18]

We begin by reconstructing the flux vector \vec{Q}_n . This vector is perpendicular to the reaction plane:

$$(1.12) \quad \vec{Q}_n = \begin{pmatrix} Q_x \\ Q_y \end{pmatrix} = \begin{pmatrix} \sum_i \omega_i \cos(n\phi_i) \\ \sum_i \omega_i \sin(n\phi_i) \end{pmatrix},$$

where the sum goes over i of every channel of the detector, ω is the multiplicity of every channel, and n is the harmonic given by the Fourier expansion. [9]

Once we have the \vec{Q}_n , we can obtain the Ψ_n following the equation:

$$(1.13) \quad \Psi_n = \frac{\tan^{-1} Q_y}{n} \frac{Q_x}{Q_x}$$

This method was introduced in 1985 [7], it has proved to be successful for experiments of heavy ions, such as ALICE (A Large Ion Collider Experiment) from the LHC, RHIC (Relativistic Heavy Ion Collider), STAR (Solenoidal Tracker at RHIC), AGS (Alternating Gradient Synchrotron, and SPS (Super Proton Synchrotron).

THE NICA AND THE MPD EXPERIMENT

JINR (Joint Institute for Nuclear Research) is an international intergovernmental organization, a worldwide important scientific centre, it is also an example of integration of fundamental theoretical and experimental research with development and application of the cutting edge technology and university education. [13]

Established on an agreement signed on March 26, 1956 in Moscow by representatives of the governments of eleven founding countries, with an aim of combining scientific and material potential of each nation. On February 1, 1957, JINR was registered by the United Nations. The Institute is located in Dubna, 120 km north of Moscow. [14]

2.1 The NICA project at JINR

The Nuclotron-based Ion Collider Facility (NICA) is a new accelerator complex at the Joint Institute for Nuclear Research (JINR) in Dubna, Russia. Its goal is to study the properties of dense baryonic matter.

The most important problems in this area are: the nature and properties of strong interactions between elementary constituents of the Standard Model of particle physics – quarks and gluons. The search for signs of the phase transition between hadronic matter and QGP; search for new phases of baryonic matter study of basic properties of the strong interaction vacuum and QCD symmetries. [5]

NICA will provide variety of beam species ranged from protons and polarized deuterons to very massive gold ions. Heavy ions will be accelerated up to kinetic energy of 4.5 GeV per nucleon, the

protons – up to 11 GeV. The heart of the NICA complex is the upgraded accelerator "Nuclotron" (that has been working at JINR since 1993). The two interaction points are foreseen at the NICA collider rings: one for heavy-ion studies with the MPD detector and another for polarized beams for the SPD experiment. [13]

NICA will have three experiments (or detectors):

1. The Baryonic Matter at Nuclotron (BMN)
2. The Spin Physics Detector (SPD)
3. The MultiPurpose Detector (MPD)

Nuclei are a bound state of protons and neutrons which are called nucleons. Nucleons are formed by quarks which interact strongly and are confined. This means that particles with color charge, such as the quarks, can't be observed in isolation. This is the reason why the study the internal structure of hadronic matter is complicated. Yet, the quark-gluon plasma (QGP) is a state of strongly interacting matter which consists in quarks and gluons which are not confined.

This state of matter could be found in the conditions of temperature and density that existed shortly after the Big Bang, at high temperature and/or density. QGP has been created in some laboratories at different conditions. In Figure 2.2 a phase diagram of hadronic matter and QGP is shown. There is a critical point in the temperature T_c from which quarks and gluons are not confined. In the same way there is a critical point N_c for the baryonic density from which quarks and gluons are not confined. The curved line in between the critical points makes reference to the phase transition between the states of strongly interacting matter; this is one of the main reasons to construct experiments in laboratories such as NICA. [15]

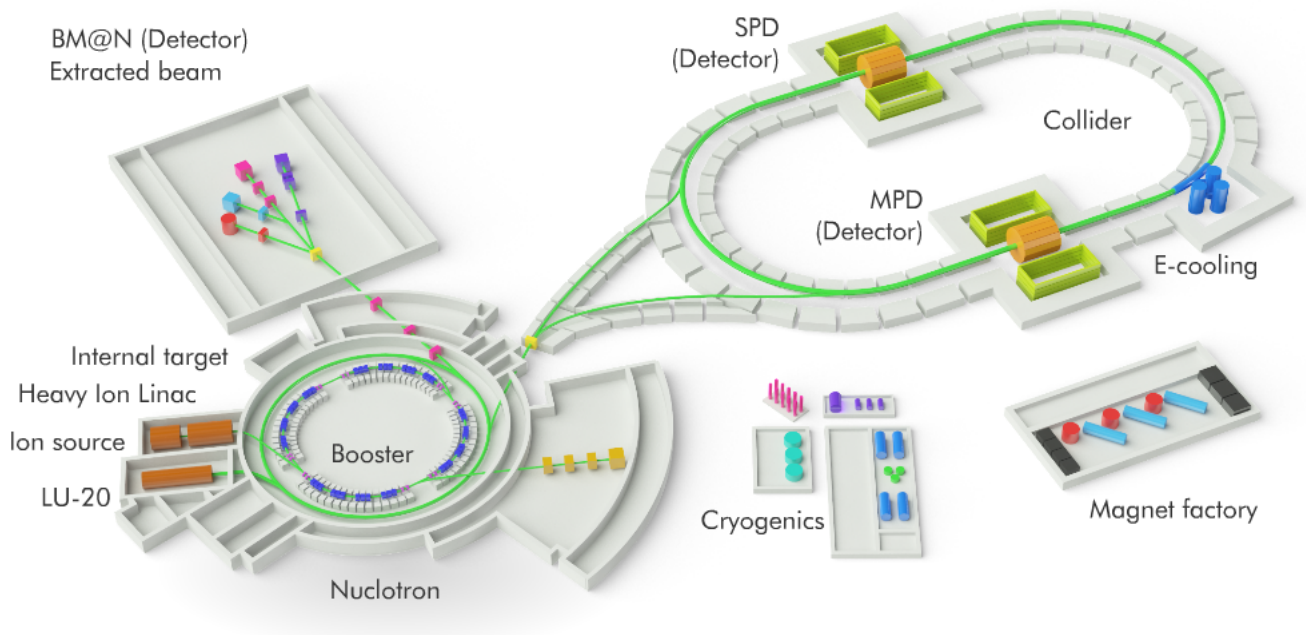


Figure 2.1: A picture of NICA. It is shown the three experiments and the rest of the components. Image taken from <http://nica.jinr.ru/complex.php>

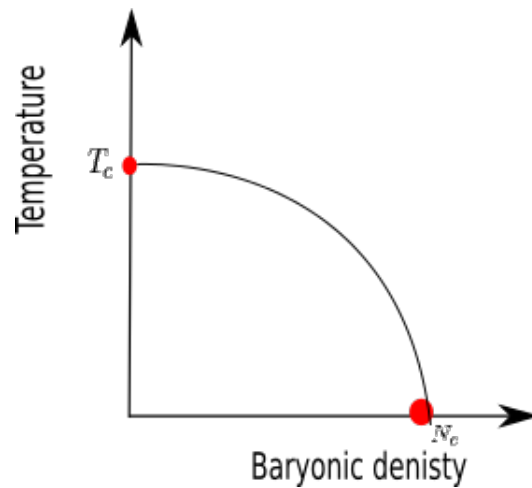


Figure 2.2: Phase diagram of hadronic matter and QGP. There is a critical point in the temperature T_c in which the quarks and gluons are not confined. In the same way there is a critical point N_c for the baryonic density from which quarks and gluons are not confined. The curved line between the critical points refers the phase transition between these both states.

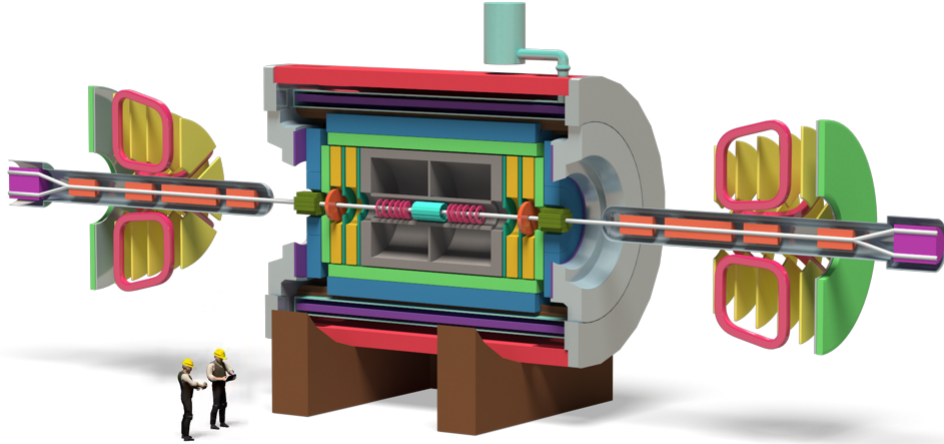


Figure 2.3: A picture of MPD. Image taken from <http://nica.jinr.ru/complex.php>

2.2 The MPD experiment

The MPD apparatus has been designed as a spectrometer capable of detecting charged hadrons, electrons and photons using heavy-ion collisions at high luminosity in the energy range of the NICA collider. To reach this goal, the detector will comprise a precise 3-D tracking system and a high-performance particle identification (PID) system based on the time-of-flight measurements and calorimetry. The basic design parameters have been determined by physics processes in nuclear collisions at NICA and by several technical constraints guided by a trade-off of efficient tracking and PID against a reasonable material budget. At the design luminosity, the event rate in the MPD interaction region is about 6 kHz; the total charged particle multiplicity exceeds 1000 in the most central Au+Au collisions at $\sqrt{S_{NN}} = 11 \text{ GeV}$. As the average transverse momentum of the particles produced in a collision at NICA energies is below $500 \text{ MeV}/c$, the detector design requires a very low material budget. The general layout of the MPD apparatus is shown in Figure 2.4. The whole detector setup includes Central Detector (CD) covering ± 2 units in pseudorapidity (η). [1]

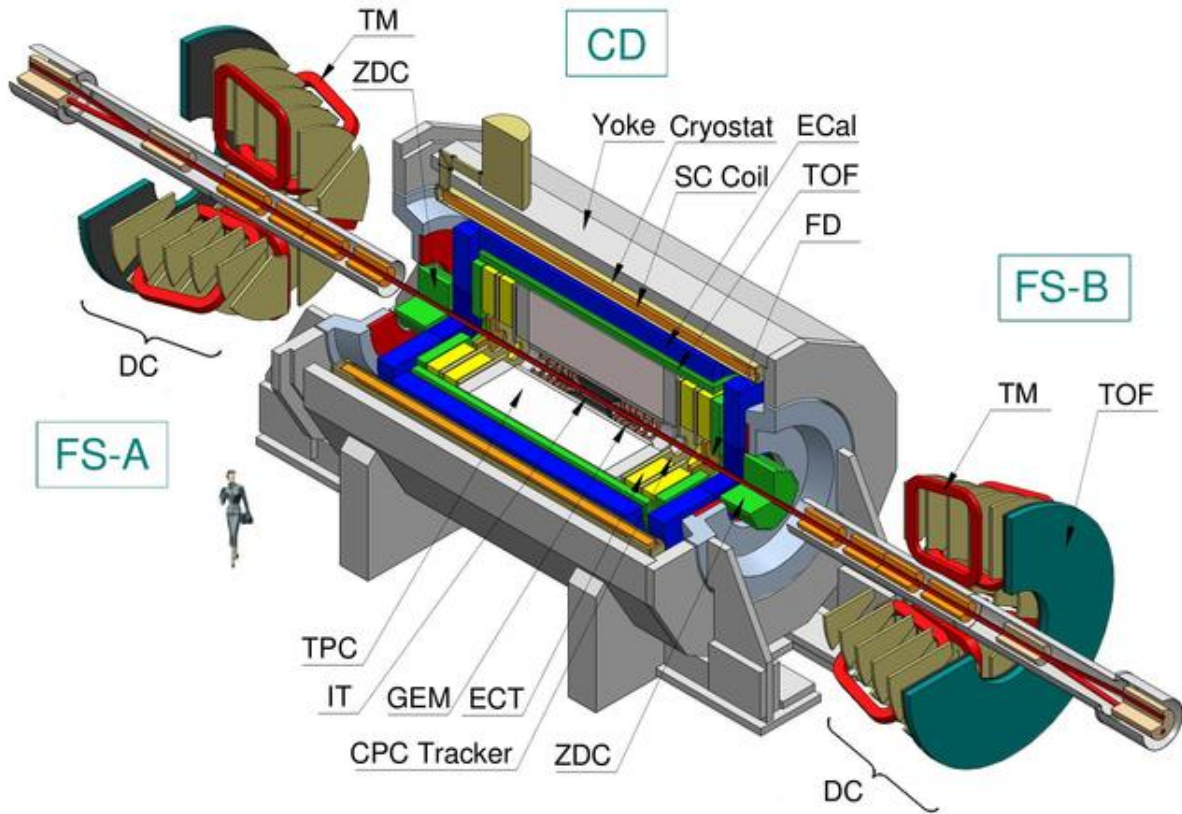


Figure 2.4: General view of the MPD-NICA <http://nica.jinr.ru/complex.php>

2.3 The Beam Monitoring Detector

2.3.1 The MexNICA collaboration

To make the MPD measurements more accurate, a new detector is proposed: The BEam-BEam monitoring detector (BE-BE), which will consist of two scintillator detectors. The main goal of this detector is to provide a fast level 0 trigger signal for MPD. Furthermore, BE-BE is suitable for:

- Optimization of events: event plane resolution
- Centrality: interaction point location
- Multiplicity reference estimator
- Trigger system
- Beam monitoring

- Discriminate centrality events from background an beam-gas interaction.
- Determinate the absolute cross section of reaction process.

The MexNICA group is a consortium conformed by students and researchers of six Mexican Universities and Institutes. The goal of the MexNICA group is to make a contribution to the MPD-NICA experiment with the design and construction of the BE-BE detector consisting of two pieces, each one located 2 meters apart on both sides of the interaction point along the beam pipe. [5]

2.3.2 Geometry

The proposal for the BE-BE for the MPD-NICA Collaboration was based in a previous version, consisting of tree rings of a granular hexagonal plastic scintillators array and light sensors, and two rings circular array of plastic scintillators, called Hybrid Geometry. Currently the proposal consists of an array of granular hexagonal plastic scintillators and light sensors, called Hodoscope Geometry. Also, the BE-BE detector will consist of two detectors located at a distance of 2 meters, on each side of the interaction point of the MPD. The pseudorapidity coverage of BE-BE would be $1.69 < |\eta| < 4.36$. In Figure 2.5, it is shown the proposed Hybrid geometry for the BE-BE detector, in Figure 2.6, the Hodoscope geometry for the BE-BE.

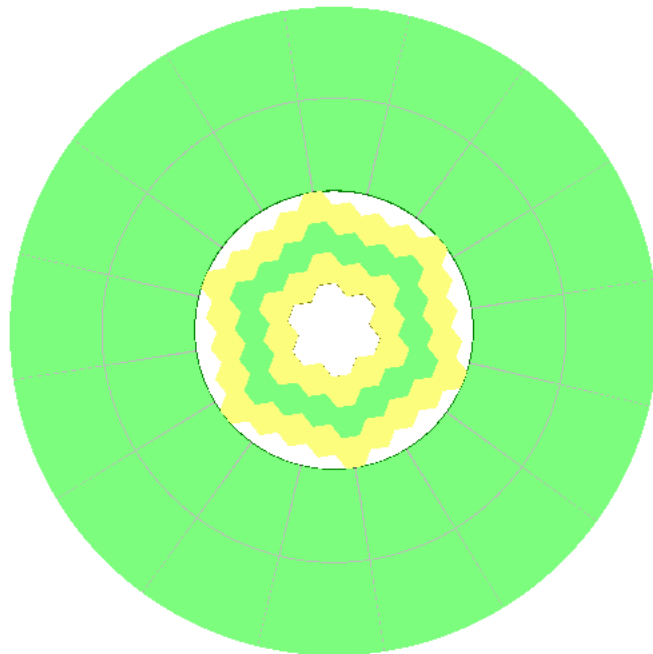


Figure 2.5: The Hybrid detector geometry

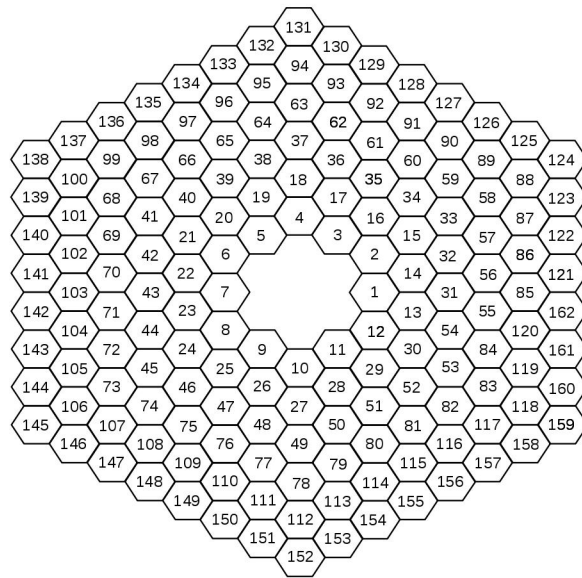


Figure 2.6: The Hodoscope detector geometry

SOFTWARE FOR THE ANALYSIS

In high energy physics, the use of sophisticated software is indispensable for the information management and data analysis.

There are two kind of data analysis in HEP: online and offline. The online analysis, monitors and analyses the first data obtained by the experiment at the moment of the collision, in the other hand, the offline, analyses the data after it is generated and reconstructs the events.

This virtual laboratory has packets of event generators, transport for the particles detector, and the geometry of them. This software construct the events by using theoretical models that need to be proved and compared with the real data of the experiments; with it, a complete analysis can be done and the event reconstruction.

For this thesis, the offline tools were used to determine, the *event plane*.

3.1 ROOT

This framework is well accepted by the experimental data analysis, due to the characteristics that it poses:: the generation of events, detector simulation, data reconstruction, data storage, data analysis and visualization.

It was constructed in 1995, its principal purpose was to be a tool for for heavy ion experiments. The root platform acquired the most important tools from the old FORTRAN, and has become now days and essential software for High Energy Physics.

The MPD-NICA collaboration has adopted ROOT as their principal system for data acquirement,

simulation and analysis. It is a software that is developing.

3.2 MPD-ROOT

Many experiments had develop their own root. As example, we can mention STAR with the implementation of the *Star Class Libraries*, and the ALICE experiment of the LHC, that made a extended version and more complete platform, called *AliRoot*.

Currently the NICA collaboration is creating the MPDRoot and SPDRoot platforms for the analysis and simulations of the future NICA complex. [12].

3.3 Macro

For calculus of Q_x and Q_y , we remember the Q_n vector is defined by:

$$(3.1) \quad \vec{Q}_n = \begin{pmatrix} Q_x \\ Q_y \end{pmatrix} = \begin{pmatrix} \sum_i \omega_i \cos(n\phi_i) \\ \sum_i \omega_i \sin(n\phi_i) \end{pmatrix}$$

Where i is the number of cell of the detector, ϕ_i is azimuthal angle of each cell, measured from the center of the detector to the center of each cell. Also ω_i is the weight given by the multiplicity in every cell. A multiplicity analysis was made in order to understand the the BE-BE's behavior.

We get Ψ_{BB} :

$$(3.2) \quad \Psi_{BB} = \frac{1}{n} \tan^{-1} \frac{\sum_i^m \omega_i \sin(n\phi_i)}{\sum_i^m \omega_i \cos(n\phi_i)}$$

In the Appendix we show a link to the macro for the analysis.

For this work we made a multiplicity analysis to BE-BE. Then the determination of the Event Plane resolution.

4.1 Multiplicity

A sample of 98000 minimum bias events of Au-Au collisions at $\sqrt{s_{NN}} = 11 \text{ GeV}$ has been simulated using the Ultra-relativistic Quantum Molecular Dynamics model (UrQMD) within the MpdRoot framework. The UrQMD [19] is microscopic many body approach which simulates multiple particle interactions, the excitation and fragmentation of colour strings and the formation and decay of hadron resonances in p-p, p-A and A-A collisions. It is based on the co-variance propagation of all hadrons on classical trajectories in combination with stochastic binary scatterings, color string formation and resonance decay. The TPC detector and the BE-BE detector has been included in the simulations. The produced particles has been propagated through the detectors using GEANT3 as transport package.

In Figure 4.1 we show the particles that "hit" the detectors are in light blue, the BE-BE is located at $Z=200$ and $Z=-200$. The lines shown at $Z=400$ and $Z=-400$ belong to the NICA Calorimeter.

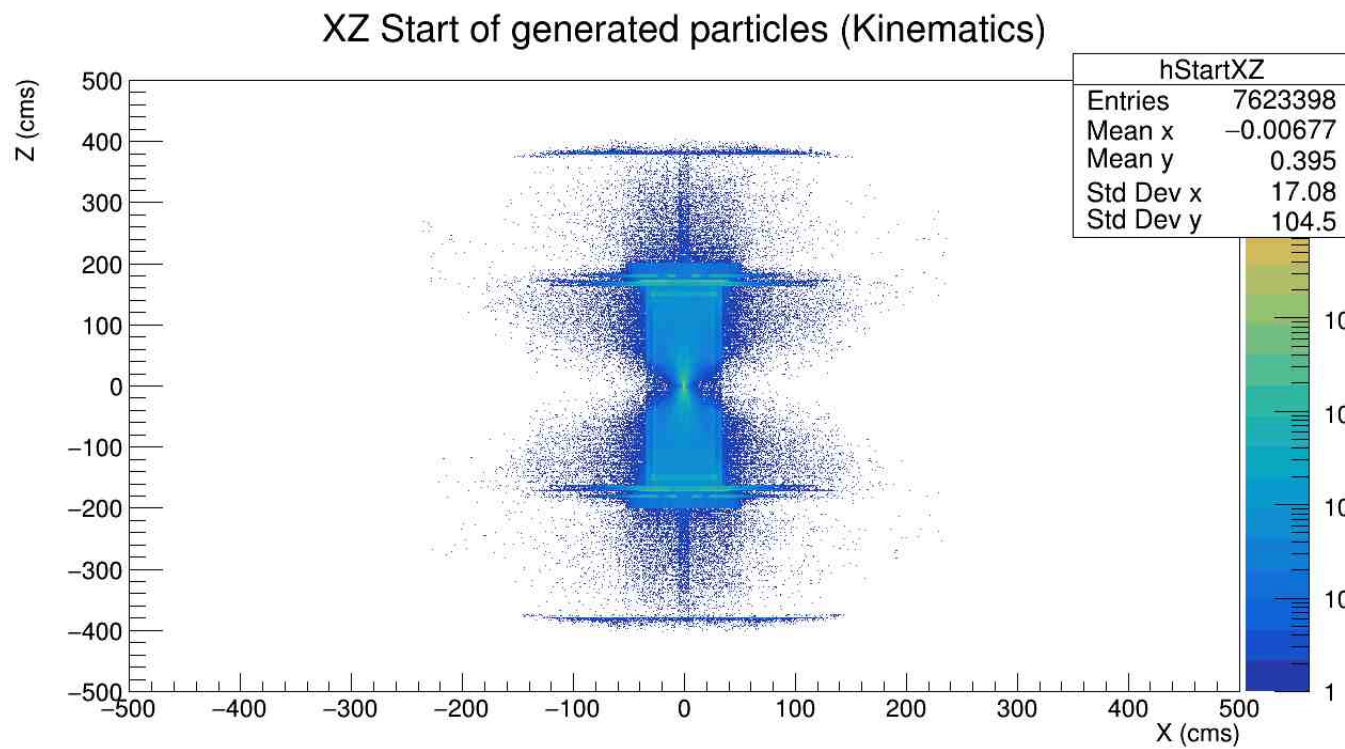


Figure 4.1: This figure shows the distribution of Kinematics, at the simulation with the BE-BE detector at both sides of the interaction point.

Hybrid Geometry

For the hybrid Geometry, the figure 4.2 a) shows, the Hits distribution of the detector for all the particles generated, and in Figure 4.2 b) only primaries.

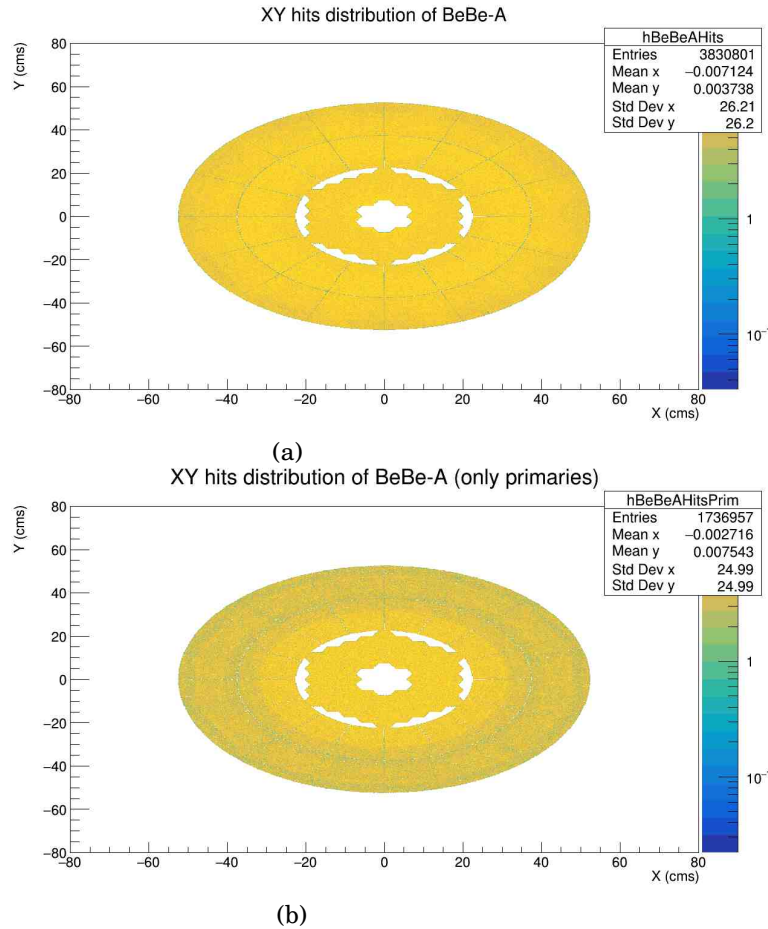
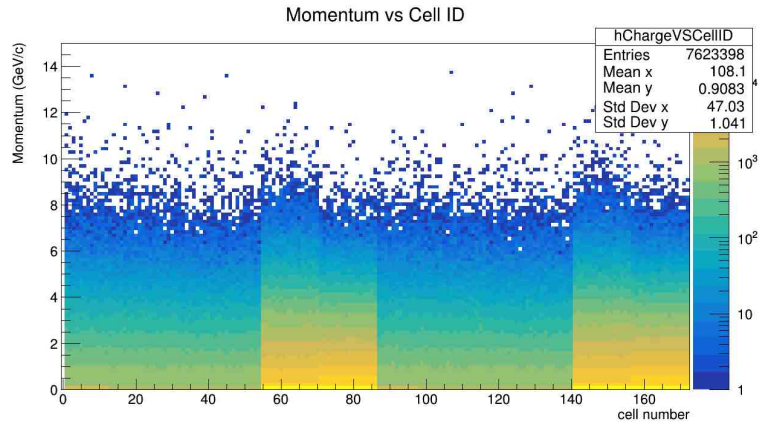
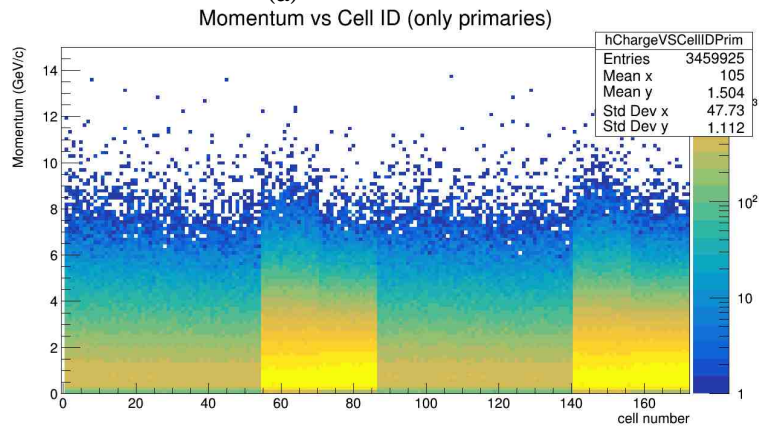


Figure 4.2: a) Hits Distribution for all the particles. b) Hits distribution only for primaries

In Figure 4.3 we show the plot of Momentum vs Cell ID of all the particles a), and only primaries the graph b). The change of color refers to the energy distribution, within the yellow areas we found more energetic particles, which we can see are collected in the outside rings, not in the inner ones. In the analysis for the primary particles we can see a larger area covered in yellow for the outer side of the detector, that means the most energetic particles will be collected in this areas.



(a)



(b)

Figure 4.3: a) Momentum vs CellID for all the particles. b) shows Momentum vs CellID only for primaries

In Figure 4.4 we have the Time vs CellID plot. This analysis was made using the number of cell of the detectors, however, as we can see there it is the same as doing the analysis from the innermost ring to the outer ring.

For primary particles the most probable value for their time of flight is around 6.5 ns with a little tail, which grows at the end of the outside most rings. In the first plot, we show that with all the events simulated, we found the presence of background all over the detector.

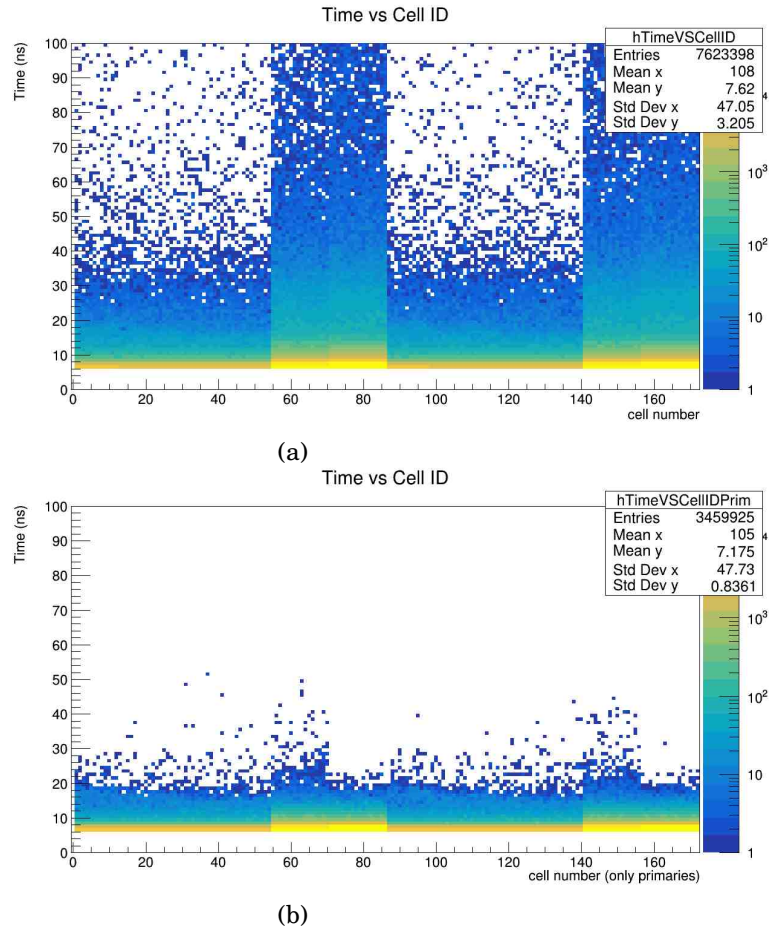


Figure 4.4: The a) plot shows the Time vs Cell ID for all the particles. The b) plot shows only for primaries

In Figure 4.5, we have the multiplicity from innermost ring to the outermost ring, this plot is the multiplicity against the CellID. We show that for the first part of the plot (corresponding to the "hexagons based" part of the detector), second part corresponds to the "circular" cells of the detector, this multiplicity is higher and has a little tail at the end. The third and the fourth are the same as the first two, because they correspond to the second part of the BE-BE (side C), which is something we would expect since both sides A and C, are the same geometry.

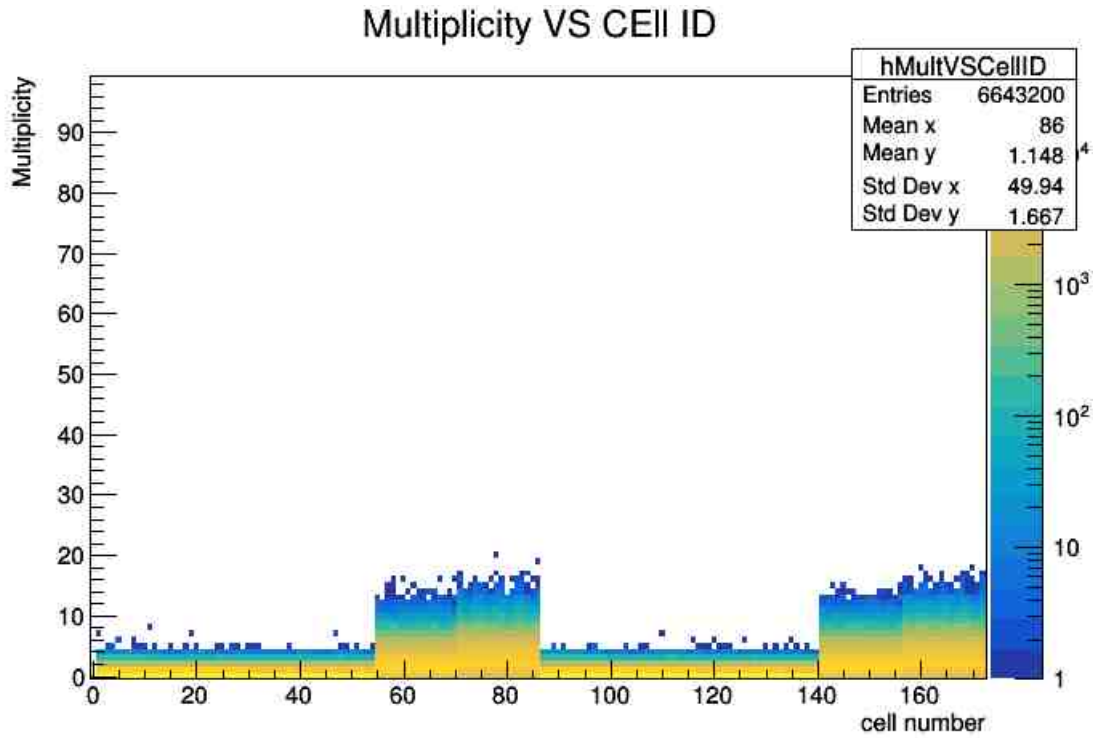


Figure 4.5: Multiplicity VS Cell ID

Figure 4.6 shows the multiplicity per ring vs the number of entries in each ring. This plot shows only results for one side of the BE-BE. The Figure 4.6 a), shows the plots overlapped, so we could see the similarities of the results. This results match the previous information obtained, since the inner hexagonal rings of the detector have similar multiplicities, but they are different from the two outside rings, this two last rings have a significantly bigger multiplicity that the inner rings.

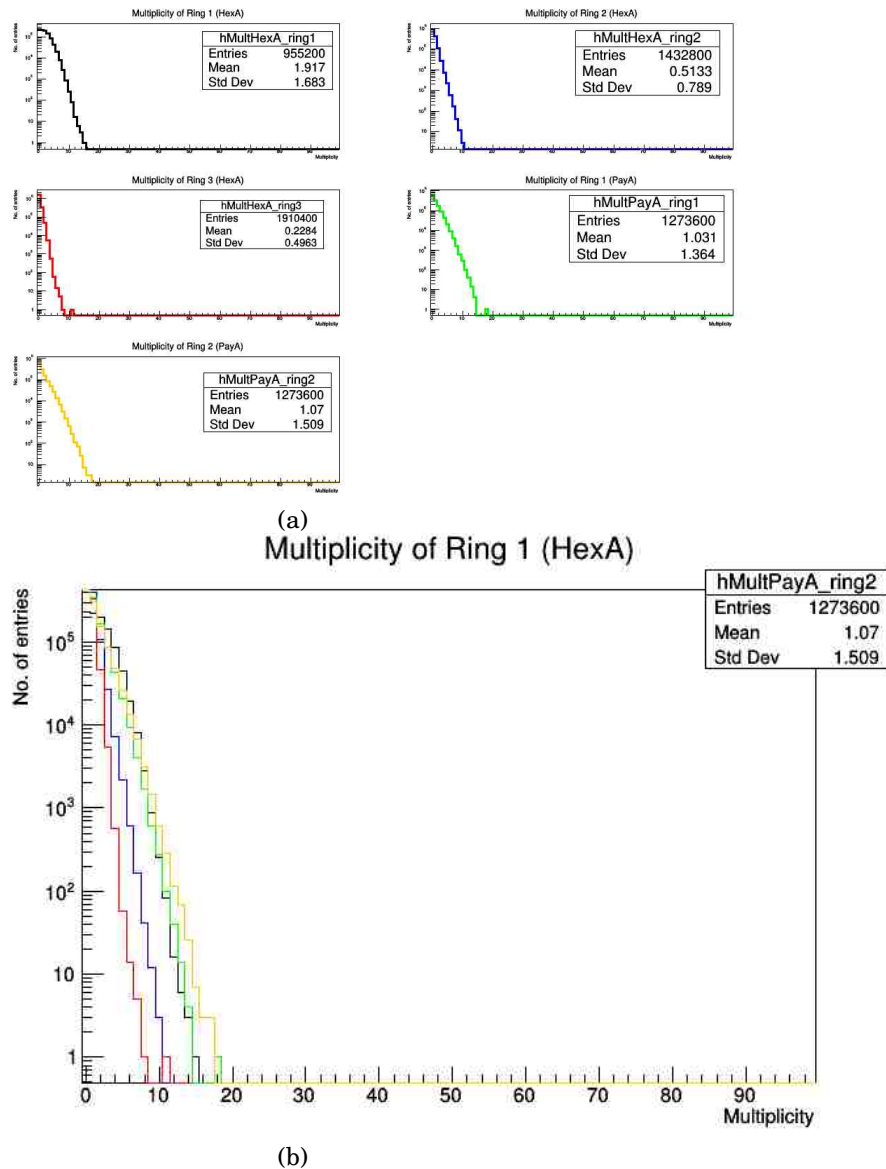


Figure 4.6: The a) plot shows a graph of Number of entries vs Multiplicity of each of the rings of the Hybrid proposal. The b) plot shows the Number of entries vs Multiplicity for each ring independently.

4.1.1 Hodoscope Geometry

For the Panal geometry, we see in Figure 4.7 a), the Hits Distribution of the Detector for both sides of it for all the particles generated, and in Figure 4.7 b) for primaries.

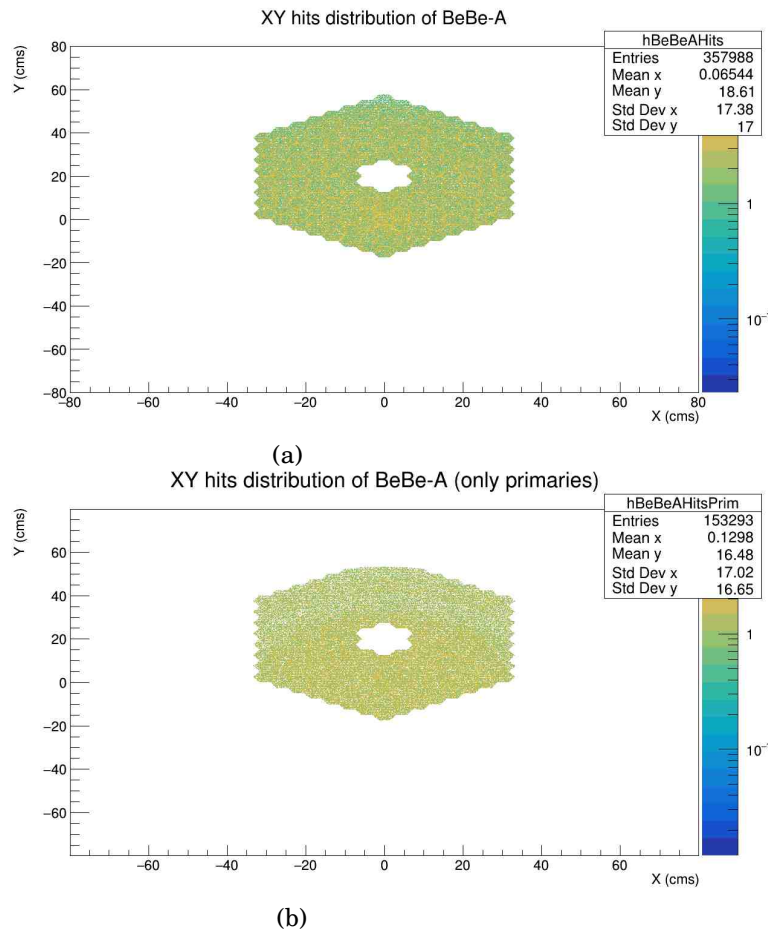


Figure 4.7: a) Shows the Hits Distribution for all the particles. b) Shows only for primaries

In Figure 4.8 are the plots of Momentum vs Cell ID of all the particles on a), and for primary particles on b). This results show us that near the center of the detector we found more energy collected.

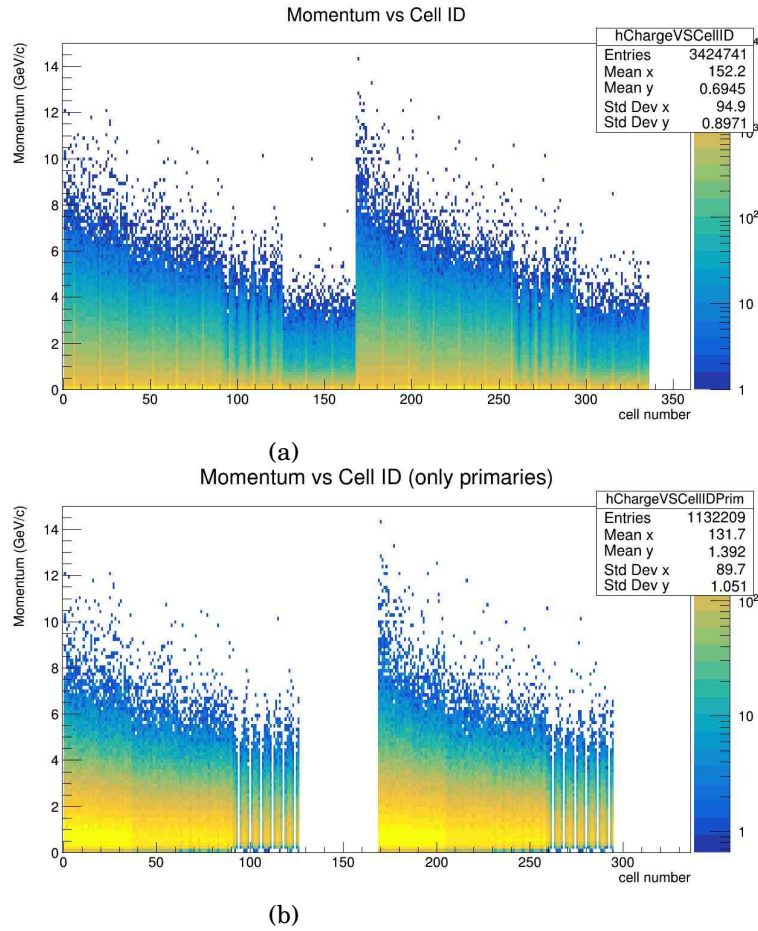


Figure 4.8: The a) plot shows the Momentum vs CellID for all the particles. The b) plot shows only for primaries

In Figure 4.9 we have the Time vs CellID. This analysis was made using the number of cell of the detectors.

In the primaries particle analysis we see that the most probable value for the time of fly is around 6.5 ns with a tail much smaller that the analysis made for the hybrid geometry, which does not exist at the end of the outside most rings, but grows near the first third area of the detector. At the first plot, we see that with all the events simulated, we found the presence of background.

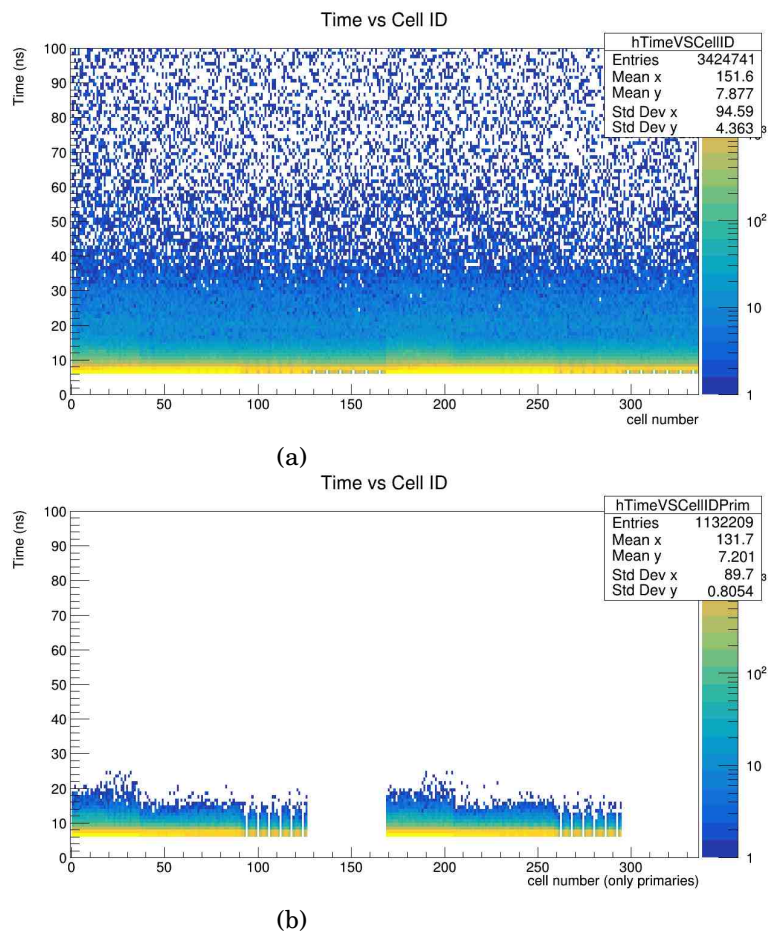


Figure 4.9: The a) plot shows the Time vs Cell ID for all the particles. The b) plot shows only for primaries

In Figure 4.10, is the multiplicity vs CellID from innermost ring to the outermost ring.

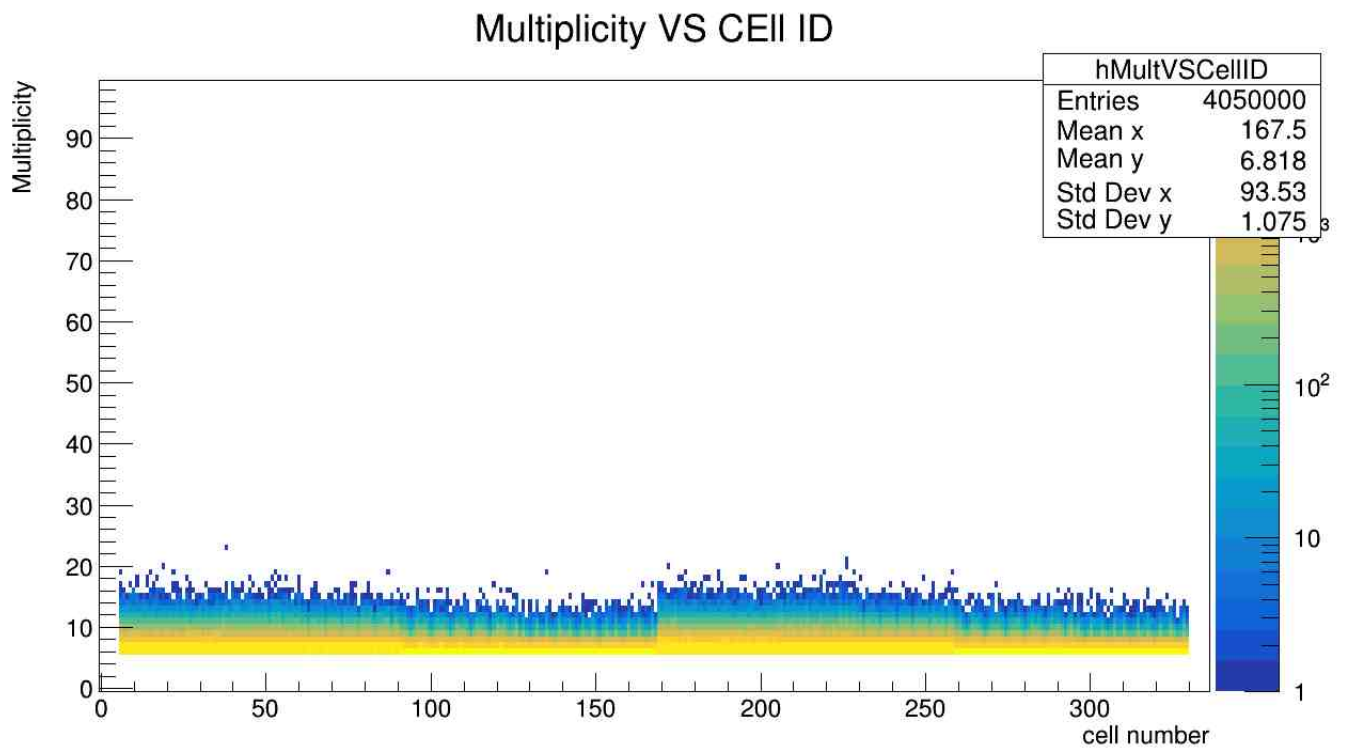


Figure 4.10: Multiplicity VS Cell ID

Figure 4.11 shows the multiplicity per ring vs the number of entries. In this plot we show that the multiplicity on every ring is really similar all over the detector.

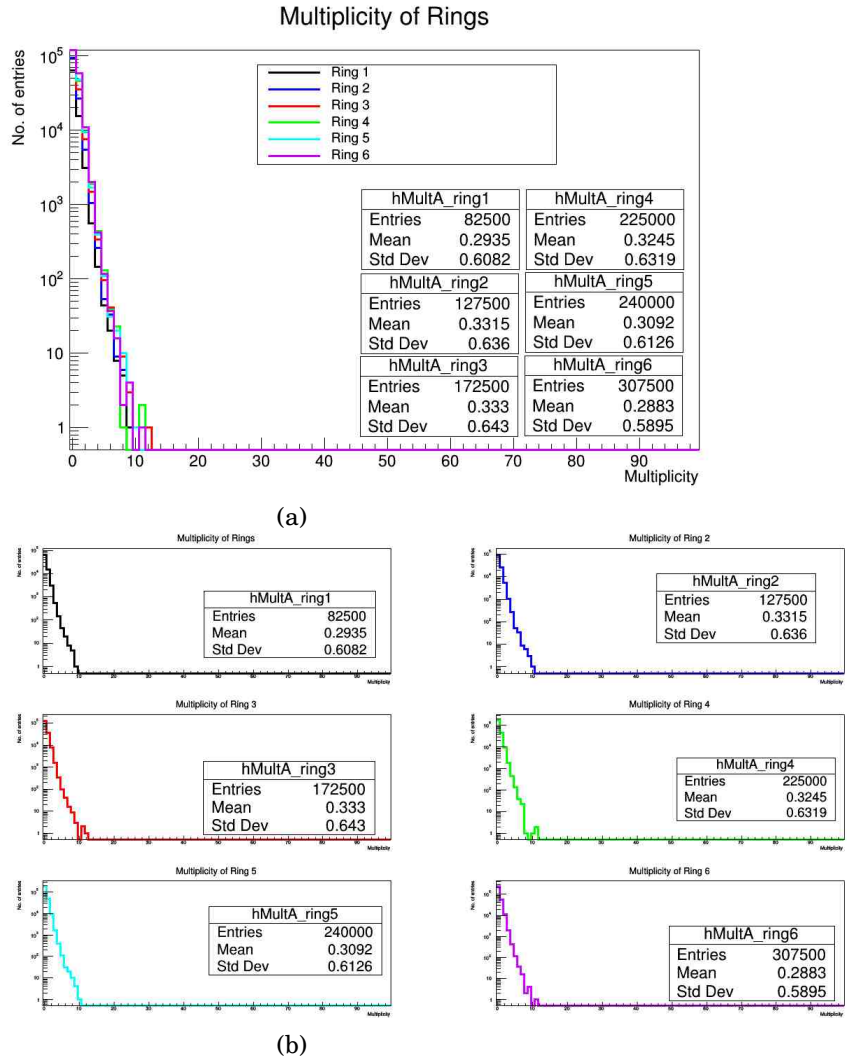


Figure 4.11: The a) contains all the plots of each of the rings of the Hodoscope Geometry proposal, all the six of them are overlaped. b) Contains the same plots but shown individually.

4.2 Event plane

To estimate the event plane resolution with the proposed BE-BE detector geometry, we simulated 95,000 Au+Au collision events using the UrQMD model [19]. This model simulates multiple particle interactions, the excitation and fragmentation of colour strings and the formation of decay of hadron resonances in p-p, p-Au and Au-Au collisions. It is based on the covariance propagation of all hadrons on classical trajectories in combination with stochastic binary scatterings, color string formation and resonance decay. A value of $n = 1$ was assumed during the simulation of the particle flow with $\sqrt{s_{NN}} = 9\text{GeV}$. The simulation was performed with the MPD-ROOT offline framework including the MPD-TPC detector and BE-BE. The produced particles were propagated through the detectors using GEANT-3 as transport package. The multiplicity per cell, ω_i was

estimated at hits level.

4.2.1 Vector Q calculus

As it was stated, the calculus of the vector Q was done using:

$$(4.1) \quad \begin{pmatrix} Q_x \\ Q_y \end{pmatrix} = \begin{pmatrix} \sum_i \omega_i \cos(n\phi_i) \\ \sum_i \omega_i \sin(n\phi_i) \end{pmatrix}$$

where ω_i is the multiplicity obtained in the simulation, and i is the number of cell assigned. ϕ is the azimuthal angle of the detector. We set ϕ of every cell to obtain Q_x and Q_y in each cell as shown in the figure.

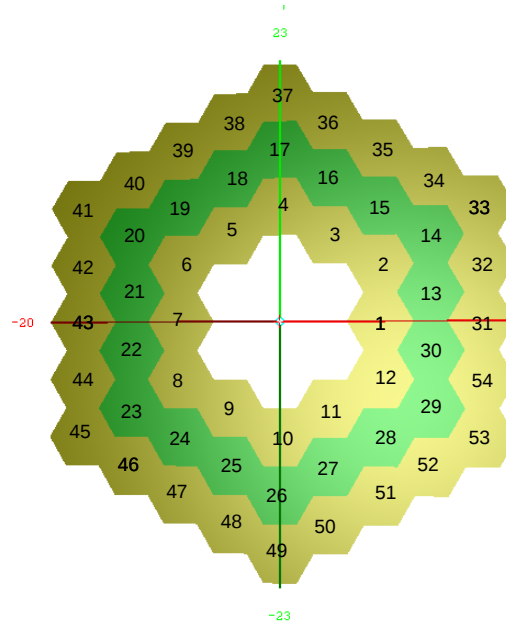


Figure 4.12: The first three rings of the BE-BE detector with the Cell ID.

To obtain the Resolution of the event plane, this work was done by comparing also with the event centrality. The cuts of the centrality used indicate the kind of event corresponding to every rate.

4.2.2 Calculus of the event plane angle.

Once obtained every variable needed to fill Ψ_{BB} , with the characteristics of our detector.

We calculate:

Centrality %	Event
0-10	Ultra Central
10-20	Central
20-30	Central
30-40	Semi Central
40-50	Semi Central
50-60	Semi Pheripheral
60-70	Semi Pheripheral
70-80	Pheripheral
80-90	Ultra Pheripheral
90-100	Ultra Pheripheral

Table 4.1: Fundamental forces of nature and their classification as the S.M says

$$(4.2) \quad \Psi_{BB} = \frac{1}{n} \tan^{-1} \frac{\sum_i^m \omega_i \sin(n\phi_i)}{\sum_i^m \omega_i \cos(n\phi_i)}$$

The event plane resolution is:

$$(4.3) \quad \langle \cos[n \times (\Psi_{BB} - \Psi_{MC})] \rangle$$

Where Ψ_{MC} is the true value given by the Monte Carlo for the n^{th} order harmonic.

If more simple words, the resolution of the event plane, (how good can the BE-BE be), is the average of the cosine of the difference between the angle Ψ_{BB} the event plane angle that was obtained in this work, and the Ψ_{MC} simulated by the Monte Carlo code.

Finally, the next plot shows the dependence of the event plane resolution with the centrality percentage.

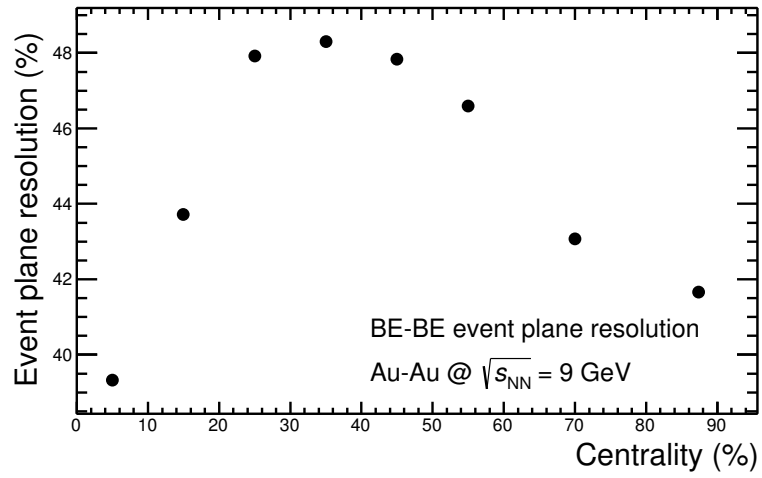


Figure 4.13: Estimated event plane resolution with BE-BE detector.

BE-BE is capable to reach a maximum of the event plane resolution for a centrality range between 25% and 45% for Au+Au collisions at $\sqrt{s_{NN}} = 9$ GeV. This effect has been reported by other experimental setups, see [6] [16].

CONCLUSIONS

The analysis made using codes in the MPD-root framework was successful. With this framework, we made a complete analysis for the Multiplicity of the detector in two of the geometries that have been proposed.

The hybrid geometry will not be the final geometry for the BE-BE detector, but the Hodoscope Geometry has shown to have more of the characteristics required for the MPD-NICA. A further analysis around the time resolution will be made by the MexNica collaboration it search for the ideal detector. This results will be arranged in an article in a near future.

This analysis was made at the level of cells, from the inner part of the detector to the outer part in the detector so the approaches of the statistics shown in this report are quite accurate.

The *event plane resolution* shows that BE-BE is a good detector for the MPD, due to the granularity and current design.

An extension for this work will be the analysis for a different n^{th} order harmonic for the calculus of Ψ_{BB} .

Something important to declare is the actual performance of the Monte Carlo implemented in the MPD-Root Framework. Since it is not completely established it causes troubles, with the generators of events. The differences in this change, are due to a mistake on the generator.

Dear reader, there is still lot work to do. We are currently working on more analysis.



APPENDIX A

In the following cernbox link you can find the codes implemented for this analysis.

<https://cernbox.cern.ch/index.php/s/fGfpB3YZV9vJesO>.

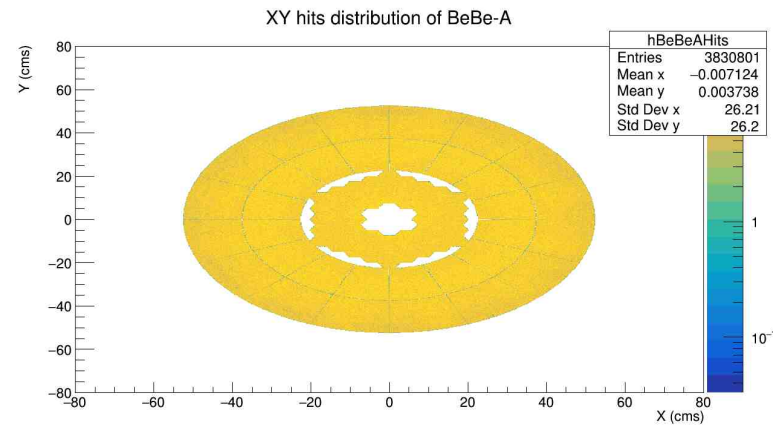
Ask for the password if needed by sending a mail to: vale.1460375@gmail.com

**APPENDIX B**

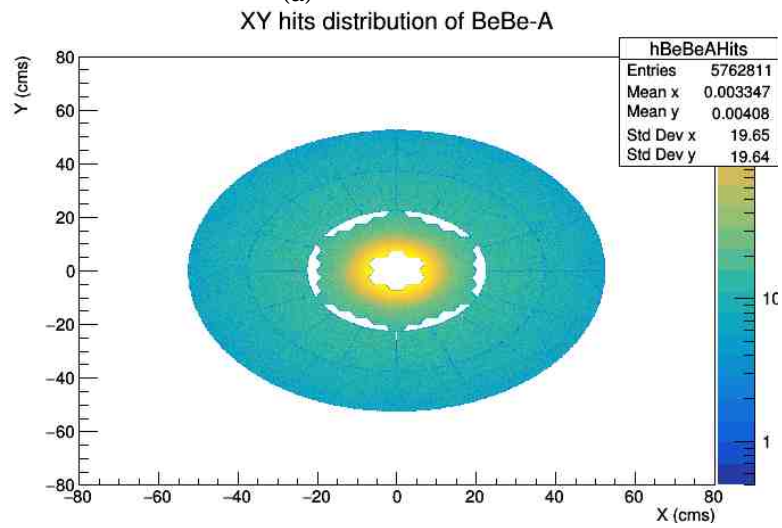
In this Appendix we show a comparison between the Multiplicity analysis done to the Hybrid Geometry on $\sqrt{S_{NN}} = 9\text{GeV}$ and $\sqrt{S_{NN}} = 11\text{GeV}$. The purpose of this appendix is to show the troubles that the generators have with the fragmentation.

And state a proof of the incorrect functioning at MPD-root functions.

In the first comparison, we see the Hits distribution for $\sqrt{s_{NN}} = 11\text{ GeV}$ and $\sqrt{s_{NN}} = 9\text{ MeV}$. It is clear that at the center of the figure A.6 b) most of the hits are at the center of the geometry. The reason that in a) the figure is almost constant all over the detector is due to the failure of the Monte Carlo implemented at MPD-root.



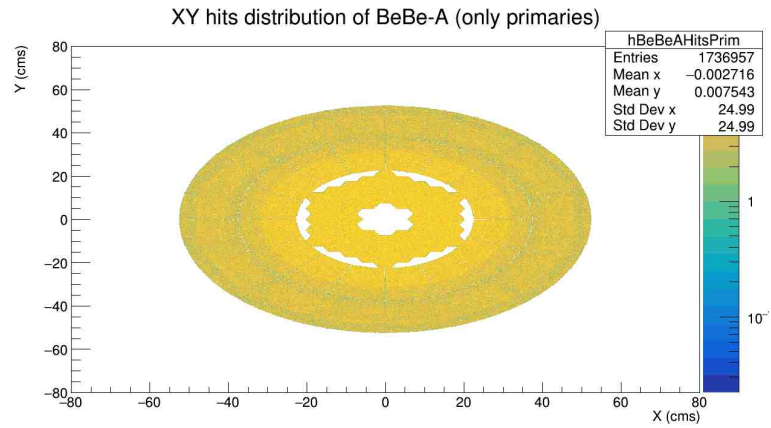
(a)



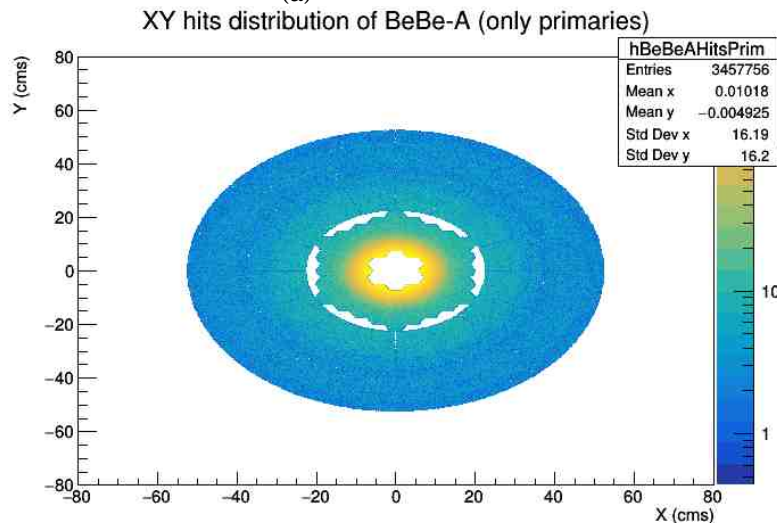
(b)

Figure A.1: a) Hits Distribution for all the particles at 11 GeV. b) Hits distribution for 9MeV.

Secondly, we compare the Hits Distribution for primary particles. The Figures show the same issue with the generators.



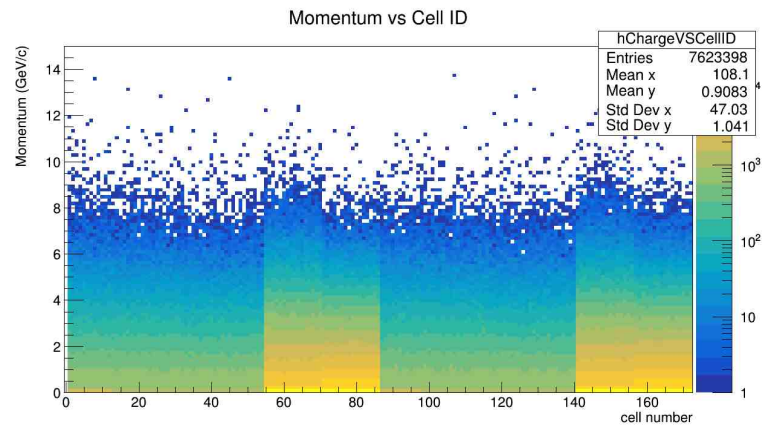
(a)



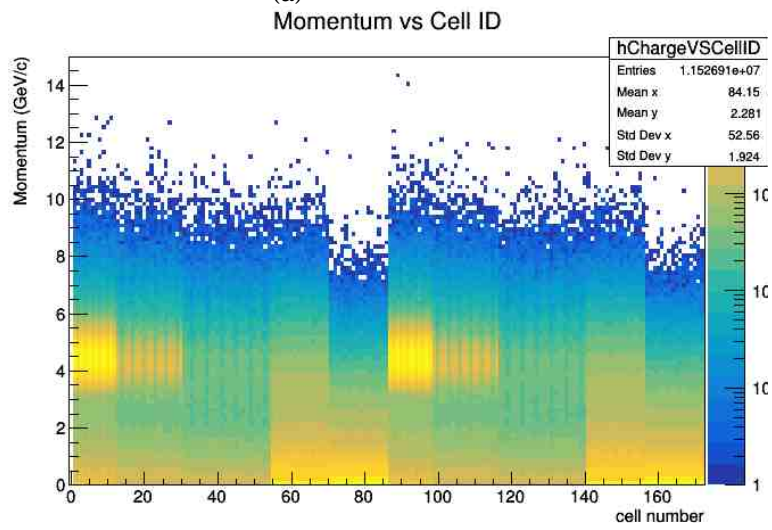
(b)

Figure A.2: a) Hits Distribution for primary particles at 11 GeV. b) Hits distribution for 9MeV.

Next, we show the momentum vs CellID comparison. Due to the fact that most of the Hits are at the center of the Geometry, there is a change on the momentum distribution.



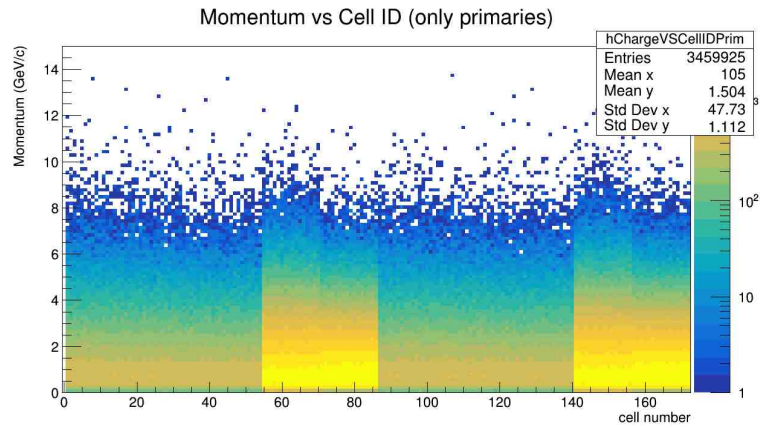
(a)



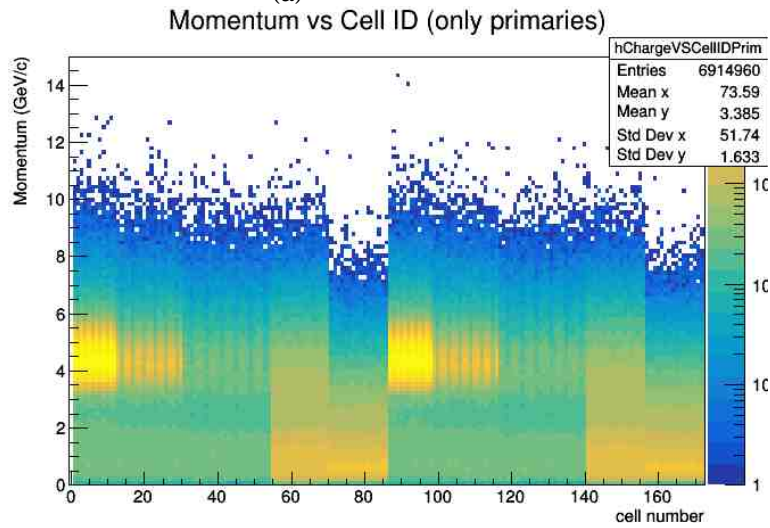
(b)

Figure A.3: a) Momentum vs CellID plot for all the particles at 11 GeV. b) for 9MeV.

For primaries, we have a similar result.



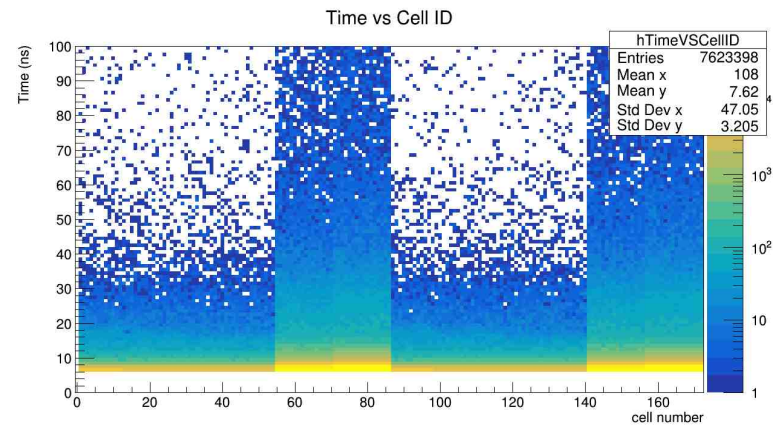
(a)



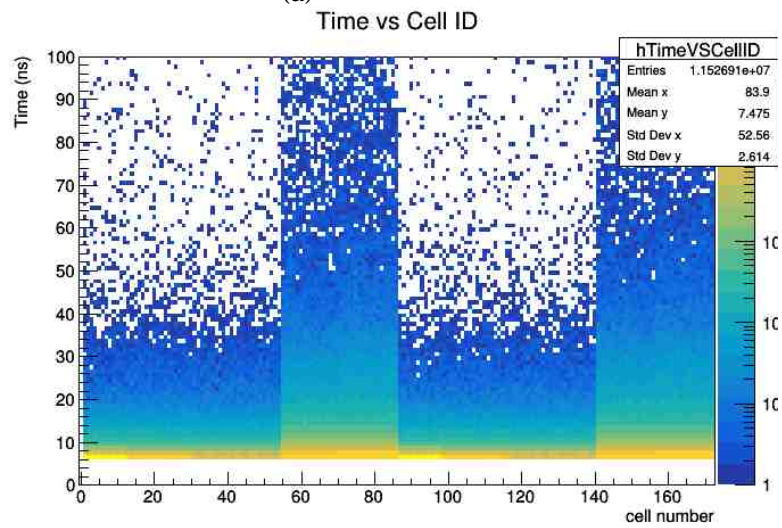
(b)

Figure A.4: a) Momentum vs CellID plot for primary particles at 11 GeV. b) Hits distribution for 9MeV.

For the Time of Flight plot, we see no changes at the shape of the plots. However the entries number is different due to the Monte Carlo tree used.



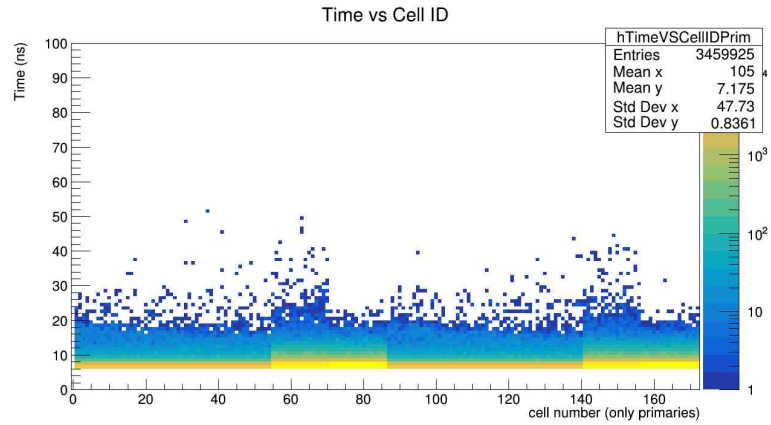
(a)



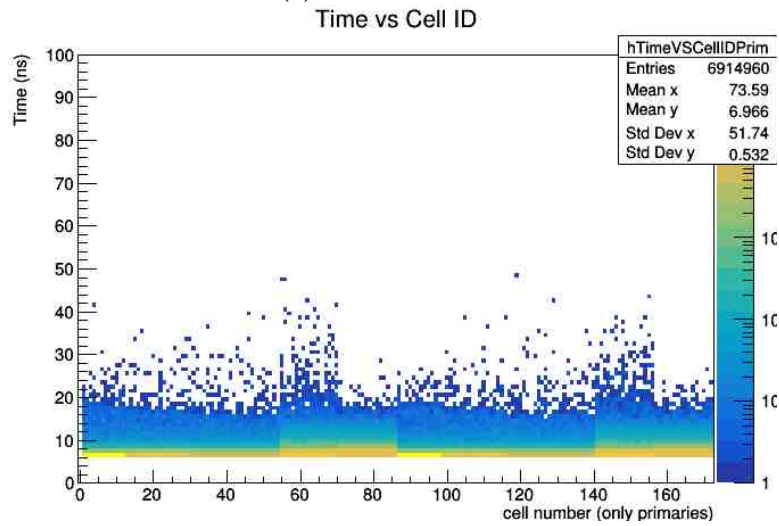
(b)

Figure A.5: a) Time of Flight plot for all the particles at 11 GeV. b) Hits distribution for 9MeV.

For primary particles, results are similar.



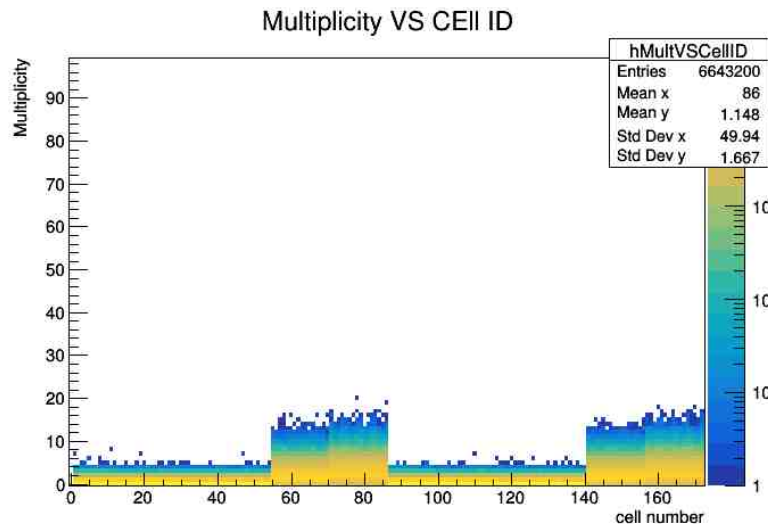
(a)



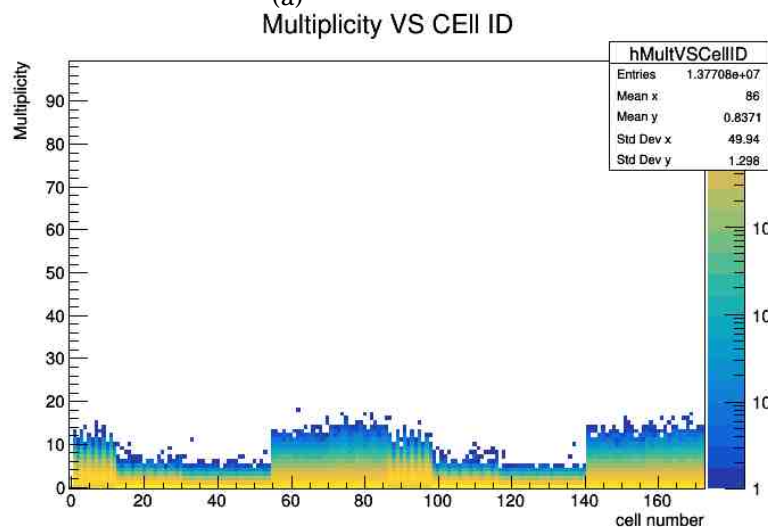
(b)

Figure A.6: a) Time of Flight plot for primary the particles at 11 GeV. b) Hits distribution for 9MeV.

Finally, the multiplicity comparison is shown in Figure A.7 where we see a little change in the first cells that correspond to the increase of hits at the first cells (first rings) of the detector.



(a)



(b)

Figure A.7: a) Hits Distribution for all the particles at 11 GeV. b) Hits distribution for 9MeV.



APPENDIX C

Arrival Time resolution measurements

In this Section we describe the results obtained by Geant4 using the hexagonal geometry. The principal goal of our detector is to reach a time resolution of 30 ps. We simulated a hexagonal scintillator material which represent the cells of Be-Be and the APDs.

From a previous result [22] it was shown that with the dimensions of the scintillator material set at $10\text{cm} \times 10\text{cm}$ and 2cm of thick. Using BC404 as the material, considering π^+ as a primary particle, and working at 5MeV and simulating 100 events; we obtained $133.579 \pm 21.803\text{ps} \leq \Delta\sigma \leq 226.409 \pm 37.821\text{ps}$. This resolution time was too big for the ideal resolution time.

So it was is natural to think that if the cell was smaller, the time resolution will be lower. Here we show the results obtained.

We made the simulations setting the hexagons dimensions at $5\text{cm} \times N\text{cm}$ and M APD's sensors at $6\text{mm} \times 6\text{mm}$ with BC404, simulating X number of events of π^+ with 5 GeV hitting at the center.

Te results found are:

Dimensions = $5\text{cm} \times 2\text{cm}$	1 sensor	2 sensors	4 sensors
BC404	44.27 ± 2.69	33.33 ± 2.93	28.02 ± 2.05
$\frac{\sigma_{\text{sensor}}}{\sqrt{M}}$		31.72 ± 2.08	22.14 ± 2.14

Table A.1: Results of σ

For this second results we also simulated the material BC422.

Dimensions = $5\text{cm} \times 1\text{cm}$	1 sensor	2 sensors
BC404	35.07 ± 4.07	35.05 ± 2.9
BC404 $\frac{\sigma_{1\text{sensor}}}{\sqrt{M}}$		24.79 ± 2.9
BC422	28.66 ± 3.44	19.88 ± 2.61
BC422 $\frac{\sigma_{1\text{sensor}}}{\sqrt{M}}$		20.26 ± 2.43

Table A.2: Results of σ

As we can see the resolution time for this arrangement is really closed to the goal of 30 ps, which is obviously very good. Unfortunately we need to cover $1\text{m} \times 1\text{m}$ of area for each side of the Be-Be detector, that means using this dimensions for the hexagons will be expensive. More results of this study will be shown in: [2].

BIBLIOGRAPHY

- [1] *The nica /mpd collaboration*, Journal of Physics G: Nuclear and Particle Physics, 36 (2009), p. 069808.
- [2] M. ALVARADO ET AL., *A beam-beam monitoring detector for the MPD experiment at NICA*, (2018).
- [3] Y. BAI, *Anisotropic Flow Measurements in STAR at the Relativistic Heavy Ion Collider*, PhD thesis, NIKHEF, Amsterdam, 2007.
- [4] W. BUSZA, K. RAJAGOPAL, AND W. VAN DER SCHEE, *Heavy ion collisions: The big picture, and the big questions*, (2018).
- [5] M. R. CAHUANTZI AND M. GROUP, *Mexnica, mexican group in the mpd-nica experiment at jinr*, Journal of Physics: Conference Series, 912 (2017), p. 012016.
- [6] S. COLLABORATION AND K. H. ACKERMANN, *Elliptic flow in au+au collisions at $\sqrt{s_n n} = 130\text{gev}$* , (2000).
- [7] P. DANIELEWICZ AND G. ODYNYEC, *Transverse momentum analisis of colective motion in relativistic nuclear collisions*, (1985).
- [8] P. D.H, *Introduction to High Energy Physics*, Cambridge University Press, 2000.
- [9] L. GONZALEZ, *Obtención del plano del evento por evento utilizando el detector V0 para el experimento ALICE del LHC*, Universidad Nacional Autónoma de México, 2012.
- [10] D. J. GRIFFITHS, *Elementary particles*, Wiley-VCH, 2008.
- [11] X.-Y. HO-KIM, QUANG. PHAM, *Elementary Particles and their interactions, concepts and phenomena.*, Springer Science, 2013.
- [12] JINR, *Mpd-root*, (2016).
- [13] ———, *Nica web page*, (2016).
- [14] ———, *Joint institute for nuclear research*, 2017.

BIBLIOGRAPHY

- [15] V. KEKELIDZE, *Nica project at jinr: status and prospects*, Journal of Instrumentation, 12 (2017), p. C06012.
- [16] V. MIKHAYLOV, A. KUGLER, V. KUSHPIL, I. SELYUZHENKOV, AND P. TLUSTÝ, *Performance study of the anisotropic flow and reaction plane reconstruction in the cbm experiment*, Journal of Physics: Conference Series, 742 (2016), p. 012023.
- [17] V. R. ORTIZ, *Final report on the summer student program*, aug 2018.
- [18] E. L. SIMILI, *Elliptic flow measurements at alice phd thesis*, Universidad de Utrecht, (2008).
- [19] ———, *Elliptic flow measurements at alice phd thesis*, Universidad de Utrecht, (2008).
- [20] B. S. SOURAV SARKAR, HELMUT SATZ, *The physics of the Quark Gluon Plasma: Introductory Lectures.*, Springer, 2000.
- [21] S. VOLOSHIN AND Y. ZHANG, *Flow study in relativistic nuclear collisions by fourier expansion of azimuthal particle distributions*, (1994).
- [22] C. H. ZEPEDA, *Final report on the summer student program*, september 2017.